JOURNAL OF BIOMOLECULAR STRUCTURE AND DYNAMICS
https://doi.org/10.1080/07391102.2020.1851303

Taylor & Francis
Taylor & Francis Group

Sensing the interactions between carbohydrate-binding agents and *N*-linked glycans of SARS-CoV-2 spike glycoprotein using molecular docking and simulation studies

Kiran Bharat Lokhande[a], Girish R. Apte[b], Ashish Shrivastava[c], Ashutosh Singh[c], Jayanta K. Pal[b], K. Venkateswara Swamy[a#] and Rajesh Kumar Gupta[b]

[a]Bioinformatics Research Laboratory, Dr. D. Y. Patil Biotechnology and Bioinformatics Institute, Dr. D. Y. Patil Vidyapeeth, Pune , Maharashtra, India; [b]Protein Biochemistry Research Laboratory, Dr. D. Y. Patil Biotechnology and Bioinformatics Institute, Dr. D. Y. Patil Vidyapeeth, Pune , Maharashtra, India; [c]Translational Bioinformatics and Computational Genomics Research Lab, Department of Life Sciences, Shiv Nadar University, G.B. Nagar, Uttar Pradesh, India

Communicated by Ramaswamy H. Sarma

ABSTRACT

A recent surge in finding new candidate vaccines and potential antivirals to tackle atypical pneumonia triggered by the novel severe acute respiratory syndrome coronavirus-2 (SARS-CoV-2) needs new and unexplored approaches in solving this global pandemic. The homotrimeric transmembrane spike (S) glycoprotein of coronaviruses which facilitates virus entry into the host cells is covered with *N*-linked glycans having oligomannose and complex sugars. These glycans provide a unique opportunity for their targeting via carbohydrate-binding agents (CBAs) which have shown their antiviral potential against coronaviruses and enveloped viruses. However, CBA–ligand interaction is not fully explored in developing novel carbohydrate-binding-based antivirals due to associated unfavorable responses with CBAs. CBAs possess unique carbohydrate-binding specificity, therefore, CBAs like mannose-specific plant lectins/lectin-like mimic Pradimicin-A (PRM-A) can be used for targeting *N*-linked glycans of S glycoproteins. Here, we report studies on the binding and stability of lectins (NPA, UDA, GRFT, CV-N and wild-type and mutant BanLec) and PRM-A with the S glycoprotein glycans via docking and MD simulation. MM/GBSA calculations were also performed for docked complexes. Interestingly, stable BanLec mutant (H84T) also showed similar docking affinity and interactions as compared to wild-type BanLec, thus, confirming that uncoupling the mitogenic activity did not alter the lectin binding activity of BanLec. The stability of the docked complexes, i.e. PRM-A and lectins with SARS-CoV-2 S glycoprotein showed favorable intermolecular hydrogen-bond formation during the 100 ns MD simulation. Taking these together, our predicted *in silico* results will be helpful in the design and development of novel CBA-based antivirals for the SARS-CoV-2 neutralization.

ARTICLE HISTORY
Received 1 August 2020
Accepted 10 November 2020

KEYWORDS
Lectin; SARS-CoV-2; spike glycoprotein; molecular docking and MD simulation; Pradimicin-A

Introduction

A recent surge in finding new candidate vaccines and potential antivirals to tackle atypical pneumonia triggered by a novel severe acute respiratory syndrome coronavirus (CoV)-2 (SARS-CoV-2) needs new and unexplored approaches in solving this global pandemic. With the unavailability of specific antivirals or vaccines against COVID-19, strategic control measures like self-distancing, strict hygiene, self-quarantine, travel restrictions and patient isolation are the few options available to avoid the spread of this infection. Therefore, in this time of crisis repurposing of existing drugs comes up as a savior. Carbohydrate-binding agents (CBAs) like plant lectins and the lectin-like non-peptidic mimic Pradimicin-A (PRM-A) have been shown to possess antiviral activity against enveloped viruses including coronavirus (Keyaerts et al., 2007; Mitchell et al., 2017; van der Meer, de Haan, Schuurman, Haijema, Verheije, et al., 2007). Lectins purified from various sources like plants, algae and cyanobacteria are known to exhibit this antiviral activity. More specifically, Mannose (Man) binding lectins like *Hippeastrum hybrid* lectin (HHA), *Galanthus nivalis agglutinin* (GNA), *Allium porrum agglutinin* (APA) and *Narcissus pseudonarcissus* agglutinin (NPA) have been shown to display antiviral activity against SARS-CoV (Frankfurt 1 strain). Similarly, *N*-acetyl glucosamine (GlcNAc) specific lectins from *Urtica dioica agglutinin* (UDA) and *Nicotiana tabacum* (Nictaba) have also been shown to have potent antiviral activity against SARS-CoV (Keyaerts et al., 2007). A red algal lectin purified from *Griffithsia* sp. known as Griffithsin (GRFT) and Cyanovirin-N (CV-N) lectin purified from *Nostoc ellipsosporum* exhibited inhibitory activity against SARS-CoV (Urbani strain) and mouse hepatitis CoV (MHV-EFLM), respectively

CONTACT Dr. Rajesh Kumar Gupta rajeshkumar.gupta@dpu.edu.in or guptarajesh76@gmail.com Protein Biochemistry Research Laboratory, Dr. D. Y. Patil Biotechnology and Bioinformatics Institute, Dr. D. Y. Patil Vidyapeeth, Pune - 411033, Maharashtra, India
#Present Address: Bioinformatics and Drug Discovery Group, MIT School of Bioengineering Science and Research, MIT Art, Design and Technology University, Pune 412201, Maharashtra, India.

Supplemental data for this article can be accessed online at https://doi.org/10.1080/07391102.2020.1851303.

(Botos et al., 2002; van der Meer, de Haan, Schuurman, Haijema, Peumans, et al., 2007). Lectin mimic of non-peptidic nature PRM-A isolated from *Actinomadura hibisca* specific for Man has also been shown to possess antiviral activity against Feline CoV serotype I strain and members of *Nidovirales* family (van der Meer, de Haan, Schuurman, Haijema, Peumans, et al., 2007). The observed antiviral activity of CBAs has been shown to depend upon the presence of Man rich *N*-linked glycans in the viral glycoproteins. For example, the addition of 1-deoxymannojirimycin which inhibits mannosidase activity in Golgi Complex and further resulted in progeny virions carrying envelop proteins having high-Man rich glycans, resulted in the enhanced antiviral activity of PRM-A towards feline infectious peritonitis virus (FIPV)-Δ3abcFL strain (van der Meer, de Haan, Schuurman, Haijema, Peumans, et al., 2007). Recently, Watanabe et al. (2020) confirmed the nature of glycans present on the S glycoprotein of SARS-CoV-2 using enzymatic digestion and LC-MS analysis. Out of the 22 *N*-linked glycosylation sites, two sites N709 and N234 were occupied by oligomannose-sugar, and specifically, the N234 site was having $Man_5GlcNAc_2$ sugar. On the other, *N*-linked glycosylation sites (N1074, N801, N717, N603, N122 and N61) complex and oligomannose types of sugars were present. In total, 8 *N*-linked glycosylation sites were reported to have prominent oligomannose types of sugars whereas the rest 14 were found to have complex sugars. Further, the glycan moiety present on the N343 site was found to be highly fucosylated. The 3D structure of SARS-CoV-2 (PDB ID: 6WPS) deposited in Protein Data Bank (PDB) also reported having GlcNAc, α-D-Man, β-D-Man and α-L-Fucose and fucosylated $Man_3GlcNAc_2$ at site N343 (Pinto et al., Preprint). In another study, (Zhou et al., 2020) analyzed the S glycoprotein secreted from the BTI-Tn-5B1-4 insect cells. Upon chymotrypsin and trypsin digestion and mass analysis, they revealed that all predicted 22 *N*-linked SARS-CoV-2 glycosylated sites are changed by high mannose *N*-glycans. S glycoprotein of the SARS-CoV-2 virus is surface exposed and is involved in virus entry into the host cells. Therefore, S glycoprotein is considered as a target of antibodies having neutralization potency and vaccine and therapeutic intervention apart from other potential targets like the main protease (Mpro), the entry receptor Angiotensin-converting enzyme II (ACE2) and the RNA dependent RNA polymerase (RdRp) (Bhardwaj, Singh, et al., 2020). The S glycoprotein of SARS-CoV-2 is also heavily glycosylated and is decorated with homogeneous and heterogeneous *N*-linked glycans, thereby providing an opportunity to target these glycans via CBAs which could serve as novel carbohydrate-based novel antivirals.

In view of the above, the major objectives of the present work was to study the interactions between carbohydrate-binding agents (CBAs) like lectins (from plants and other origins) and the lectin-like non-peptidic mimic Pradimicin-A with *N*-linked Glycans of SARS-CoV-2 spike glycoprotein using molecular docking and simulation studies. Here, in this study, we selected lectins like NPA, UDA, GRFT and CV-N, Banana lectin (BanLec) wild-type and mutant (H84T mutant) type and non-peptidic mimic PRM-A based on their previously reported antiviral activity and availability of PDB structures. We performed molecular docking of all CBAs with S Glycoprotein and analyzed their respective molecular interactions. Further, we have also performed 100 ns molecular dynamic (MD) simulation of all the CBAs with the S glycoprotein of SARS-CoV-2. In addition, we have also carried out the molecular mechanics, the generalized Born model and solvent accessibility (MM/GBSA) calculations of docked complexes (PRM-A and all the lectins with S glycoprotein of SARS-CoV-2). In our study, all the CBAs are seen to interact well with the SARS-CoV-2 S glycoprotein. More specifically, we also analyzed the BanLec mutant lectin (H84T) where replacement of histidine with threonine at 84th position in BanLec abolishes its mitogenic activity while significantly retaining its broad-range antiviral activity. Interaction of this lectin with S glycoprotein revealed that docked complexes of wild and mutant type of BanLec gave docking energy of −219.8 kcal/mol and −220.7 kcal/mol, respectively, and that the point of mutation, i.e. H84T was also seen to interact with the S glycoprotein in both the complexes. Our study, thus, showed that targeting of *N*-linked glycans of the SARS-CoV-2 S glycoprotein via CBAs could serve as an attractive therapeutic target for novel antivirals. Thus, redesigning of CBAs using simple bioengineering principles may bring these antiviral CBAs for COVID-19 therapy which is currently not available in the clinic.

Methodology

Retrieval and preprocessing of SARS-CoV-2 spike glycoprotein, Pradimicin-A and lectins from various origins

The 3-dimensional (3D) crystal structure of the SARS-CoV-2 S glycoprotein crystallized by the Cryo-electron microscopy technique (Cryo-EM) having 3.10 Å resolution, was downloaded from the PDB databank (Berman et al., 2000) with PDB ID: 6WPS (Pinto et al., 2020, Preprint). The PubChem database (Kim et al., 2019) was used to retrieve the 2-Dimensional (2D) structure of Pradimicin A (PRM-A) with PubChem CID: 5479145. Also, the various plant lectins like NPA with PDB ID: 1NPL (Sauerborn et al., 1999), UDA with PDB ID: 1EHD (Harata & Muraki, 2000), BanLec of wild-type (PDB ID: 3MIT) (Sharma & Vijayan, 2011) and H84T mutant type (PDB ID: 4PIT) (Swanson et al., 2015), lectins from algal and cyanobacterial origin like GRFT (PDB ID: 2GUD) (Ziółkowska et al., 2006) and CV-N with PDB ID: 3GXZ (Botos et al., 2002), respectively, were retrieved from the PDB databank for the macromolecular docking studies with SARS CoV-2 S glycoprotein.

The protein preparation wizard tool of Maestro software (Schrodinger Release 2020-3: Maestro) was used to prepare all the lectins and SARS-CoV-2 S glycoprotein in this study. All missing hydrogen atoms in the PDB's were added and the uncapped N-termini and C-termini were capped with ACE (*N*-acetyl) and NMA (*N*-methyl amide) groups, respectively. The 2D structure of PRM-A was converted into the 3D structure and further subjected to energy minimization to get energetically stable conformation of PRM-A using Maestro with an OPLS-2005 force field.

Table 1. The binding site residues and the glycan specificity of the lectins.

Carbohydrate-binding agents (CBAs)	Glycan specificity	Active site residues
Plant origin *Narcissus Pseudonarcissus* Agglutinin (NPA)	Mannose	Asn93, Asp91, Gln89, Tyr97, Asn30, Asp28, Gln26, Tyr34, Tyr65, Asn61, Gln57, Asp59, Trp73, Ala42, Asn44
Urtica diocia agglutinin (UDA)	*N*-acetyl glucosamine (GlcNAc)	Ser19, Tyr30, Cys24
Banana lectin (BanLec) Wild-type	Mannose/ Oligomannose	Asp35, Val36, Gly34, Asp38, Gly60, Phe131, Asp133, Gly15, Asp130, Gly105, Asn106, Ser33, His63
Mutated (H84T)		Thr84, Lys130, Phe131, Asp133, Gly15, Gly60, Asp38, Val36, Asp35
Other origins Griffithsin (GRFT)	Mannose, Glucose, *N*-acetyl glucosamine, 1-6 α-mannobiose	Tyr110, Gly108, Asp109, Gly12, Asp112, Gly44, Asp30, Tyr28, Ser27, Gly90, Asp70, Tyr68, Gly66, Asp67
Cyanovirin - N (CV-N)	α(1, 2)-mannose	Leu1, Lys3, Thr7, Asn93, Asp95, Glu23, Gly2

Defining binding site of the SARS CoV-2 S glycoprotein and lectins for macromolecular and ligand docking

To obtain structural information of SARS-CoV-2 S glycoprotein, a domain search was performed using NCBI Conserved Domain Search (Marchler-Bauer et al., 2017). The amino acid residue, i.e. Asn343, glycans like BMA1323, MAN1324, MAN1325 and NAG1321, NAG1322 of the Receptor Binding Domain (RBD) of the S glycoprotein (PDB ID: 6WPS) were defined as the binding site residues for the macromolecular (Protein–Protein) docking with lectins and ligand docking with PRM-A. The binding site residues of all the lectins which were considered for macromolecular docking are summarized in Table 1.

Molecular docking calculations (macromolecular and ligand docking)

To reveal the binding pose and intermolecular interactions of PRM-A with glycans that are present on the SARS-CoV-2 S glycoprotein, molecular docking calculations were carried out with docking program FlexX (Bursulaya et al., 2003). During FlexX Docking, the receptor is kept as rigid while the PRM-A is treated as flexible. FlexX is considered the best enrichment module in virtual screening that produces precise binding poses of the ligand within the receptor binding site. In FlexX, atomic charges were calculated using input structure and protonation state for the same were considered in an aqueous solution which is recommended by FlexX software. The FlexX gives the best-docked poses of PRM-A within the binding site of the S glycoprotein using an incremental construction algorithm (Sato et al., 2006; Singh, Bhardwaj, Das, et al., 2020). Also, the HDOCK server (Yan et al., 2020) was used for the macromolecular docking of lectins with SARS-CoV-2 S glycoprotein. Using a hybrid algorithm, the interactions between lectins and S glycoprotein were predicted by the HDOCK server. The HDOCK server implemented the global docking with the input receptor and ligand structure to sample accepted binding conformations via an FFT-based algorithm. Also, the docking program of the HDOCK executes rigid-body docking by considering both the protein and ligand (protein) onto grids (Yan et al., 2020). The binding mode of macromolecules was evaluated by the binding energy and ranked them according to their docking energies. We have taken the complexes which show the best intermolecular interactions between SARS-CoV-2 S glycoprotein and carbohydrate recognition domain (CRD) of lectins.

Molecular dynamic calculations of Pradimicin-A and all the lectins (NPA, UDA, BanLec [wild-type and mutant], GRFT and CV-N) with SARS-CoV-2 S glycoprotein

To assess the binding stability of PRM-A and all the lectins (NPA, UDA, BanLec [wild-type and mutant], GRFT and CV-N) with the binding site of SARS-CoV-2 S glycoprotein, 100 ns MD simulation for S glycoprotein-PRM-A complex and S glycoprotein-lectin complexes were carried out using the Desmond module of Schrodinger software (Schrödinger Release 2020-3: Desmond). The MD simulations give the dynamic behavior of protein upon binding of ligand or macromolecule. The complex systems, i.e. SARS-CoV-2 S glycoprotein-PRM-A and S glycoprotein-lectins were subjected to solvation and ionization using Desmond's system builder panel. The complex system was solvated by using a three-point (TIP3) water model in a 10 Å spacing cubic box with a periodic boundary condition (PBC) box (Bhardwaj & Purohit, 2020b). A total number of 81348, 82607, 81209 and 83444 water molecules were added in the complex system of SARS-CoV-2 S glycoprotein-NPA, SARS-CoV-2 S glycoprotein-BanLec (wild-type), SARS-CoV-2 S glycoprotein-BanLec (mutant) and SARS-CoV-2 S glycoprotein-UDA, respectively. While in the SARS-CoV-2 S glycoprotein-CV-N, SARS-CoV-2 S glycoprotein-GRFT and SARS-CoV-2 S glycoprotein-PRM-A complexes 83210, 81303 and 53737 water molecules were added, respectively, during the 100 ns MD simulation.

The neutralization of the solvent system was done by adding 5 Cl^- in both SARS-CoV-2 S glycoprotein-BanLec (mutant) and SARS-CoV-2 S glycoprotein-PRM-A complexes of 1.119 μM and 1.692 μM concentration, respectively, while 3 Cl^- counter ions of 0.660 μM concentration were added in the SARS-CoV-2 S glycoprotein-BanLec (wild-type) complex. 2 Cl^- were added in both SARS-CoV-2 S glycoprotein-CVN and SARS-CoV-2 S glycoprotein-NPA simulation complexes of 0.437 μM and 0.447 μM concentration while only 1 Cl^- was added to the SARS-CoV-2 S glycoprotein-GRFT of 0.224 μM concentration. In this study, energy minimization of the system was done using the steepest descent method and OPLS-2005 force field (Singh, Bhardwaj, Sharma, et al., 2020). To

define the atomic partial charges for all atoms in the system, we have used standard charges from the OPLS-2005 force field. The 100 ns MD simulation was carried out using NPT (*N* = Number of Atoms, *P* = Pressure and *T* = Temperature) ensemble at a constant temperature of 300 K.

To explore the binding stability of the complex systems, the intermolecular hydrogen bond (H-bond) interactions of PRM-A and all the lectins with SARS-CoV-2 S glycoprotein and glycans were evaluated using 1000 frames generated from 100 ns MD simulation trajectory data and was used to generate intermolecular H-bonding pattern through simulation event analysis application in Maestro. It illustrates the existence of intermolecular H-bonding between SARS-CoV-2 S glycoprotein with PRM-A and all the lectins individually during the 100 ns MD simulation. In terms of Root Mean Square Deviation (RMSD), the conformational changes of the C-α backbone atoms of the S glycoprotein were compared with the initial conformations of a crystal structure (PDB ID: 6WPS). Also, the deviation of PRM-A and all the lectins after binding with SARS-CoV-2 S glycoprotein were compared with the docked structure of PRM-A and crystal structures of all the lectins.

Binding free energy calculations

The Prime MM/GBSA (Molecular Mechanics-Generalized Born Surface Area) was performed to get binding free energies for a set of PRM-A and lectins with SARS-CoV-2 S glycoprotein. Prime MM/GBSA works with the combination of SGB solvation model for polar solvation (GSGB), nonpolar solvation (GNP), advanced OPLS-2005 force field and Molecular Mechanics Energies (EMM), that compiled different nonpolar solvent accessible surface area and van der Waals interactions while neglecting the entropy changes in resulting protein-ligand binding (Lokhande et al., 2020). The MD trajectory clustering was performed and subjected to binding free energies changes during the 100 ns MD simulation upon PRM-A and all the lectins binding with SARS-CoV-2 S glycoprotein were calculated using the following equations .

$$\Delta G_{bind} = G_{complex} - (G_{protein} + G_{ligand})$$
$$G = E_{MM} + G_{SGB} + G_{NP}.$$

Where the $G_{complex}$ represents Protein–Ligand complex energy, $G_{protein}$ is the Protein-energy and G_{ligand} is the unbound ligand energy. Also, the EMM represents molecular mechanics energies, GSGB is an SGB solvation model for polar solvation and GNP is a nonpolar solvation term (Bhardwaj & Purohit, 2020a).

Results

Structural analysis of SARS-CoV-2 S glycoprotein

The structural components of SARS-CoV-2 S glycoprotein were visualized by Maestro software. Figure 1 shows secondary structural analysis of SARS-CoV-2 S glycoprotein which contains two structurally independent domains like Receptor Binding Domain (RBD) and N-Terminal Domain (NTD) in the S1 subunit

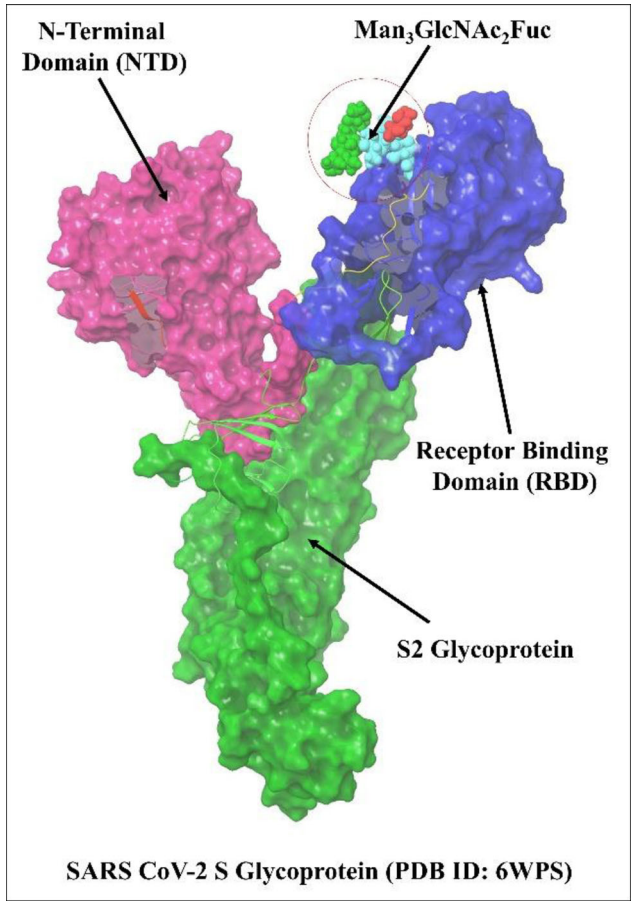

Figure 1. Illustration of SARS-CoV-2 S glycoprotein. The receptor binding domain (RBD) shown in blue surface and pink colored surface represents N-terminal domain (NTD) at the upside. The S2 glycoprotein was shown in green color. The Man (Green)-GlcNAc (Cyan)-Fuc (Red) complex represented in the CPK model on the surface of RBD.

at the upper side of S2 glycoprotein. While a hydrophobic fusion peptide and two heptad repeat regions were present in the S2 subunit. At the surface of RBD, the $Man_3GlcNAc_2Fuc$ oligosaccharide linked with residue Asn343 was present.

Besides, the RBD of SARS-CoV-2 shows notably greater binding affinity to the human Angiotensin-converting enzyme 2 (ACE2) receptor than the RBD of SARS-CoV. In this study, for docking calculations, we have defined the SARS-CoV-2 S glycoprotein binding site on the RBD of the S1 subunit.

Molecular docking

Intermolecular interactions between Pradimicin-A with SARS-CoV-2 S glycoprotein

The ligand docking was carried out to perceive the binding pose and binding affinity of PRM-A with S glycoprotein at the glycan site. The detailed interaction analysis of PRM-A with the S glycoprotein glycans along with the FlexX docking energy is summarized in Table 2. The docking result suggests that the binding of PRM-A occurred only with SARS-CoV-2 glycans without forming any bond with the protein (Figure 2(a)). The PRM-A forms five H-bonds with *N*-Acetyl glucosamine and Mannose with −11.3 kcal/mol docking energy. Figure 2(b) shows the intermolecular interactions of PRM-A with SARS-CoV-2 glycans by forming H-bonds with NAG1321, NAG1322 and MAN1325 at

Table 2. Detailed interaction analysis of Pradimicin-A with SARS-CoV-2 spike protein glycans.

CBA	PubChem CID	Docking energy (kcal/mol)	Interacting glycans	Bond type	Bond distance (Å)
Pradimicin- A	5479145	–11.3	NAG1321	H-Bond	1.71
			NAG1322	H-Bond	2.05
			BMA1323	2 H-Bond	2.13 & 2.59
			MAN1325	H-Bond	1.90

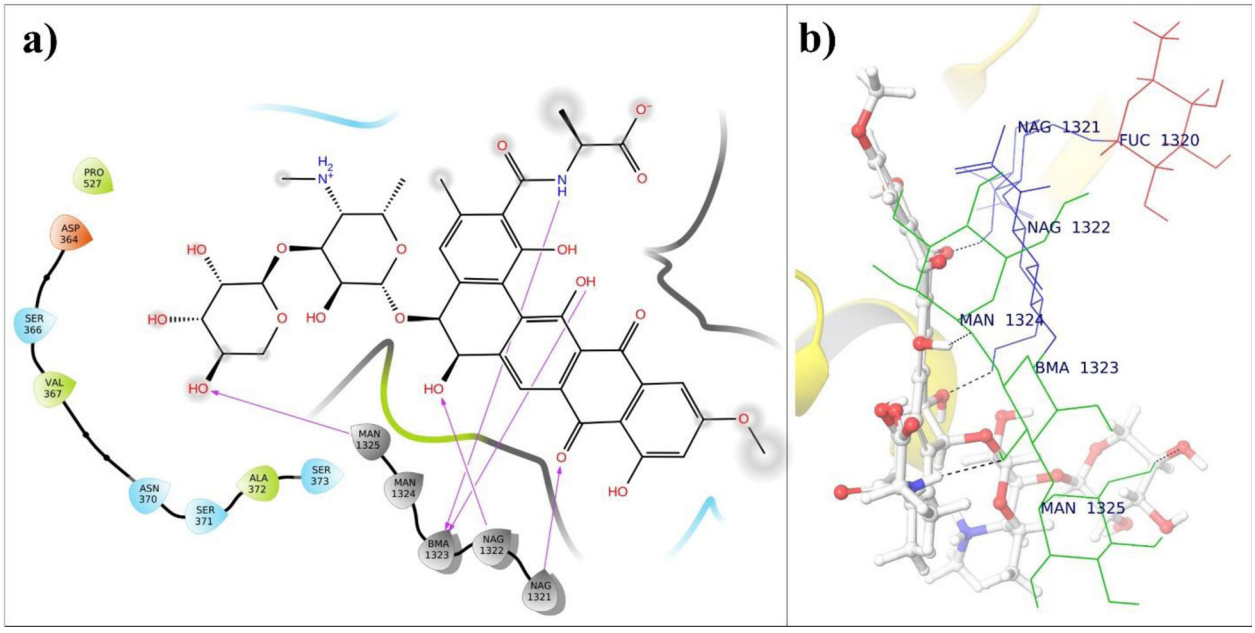

Figure 2. Binding mode of PRM-A with *N*-linked glycans of SARS CoV-2 spike glycoprotein: (a) 2D interaction diagram of PRM-A with glycan; (b) 3D intermolecular interaction between PRM-A and *N*-linked glycans of SARS CoV-2 spike glycoprotein. The SARS CoV-2 spike glycoprotein is shown in the ribbon form, PRM-A has been shown in ball and stick model and Glycans are shown in wireframe. GlcNAc, Man and Fuc are represented in blue, green and red color, respectively.

bond distances of 1.71 Å, 2.05 Å and 1.90 Å, respectively. Also, PRM-A forms two H-bonds with BMA1323 at a bond distance of 2.13 Å and 2.59 Å.

Protein–Protein interactions between lectins from various origins with SARS-CoV-2 S glycoprotein

We have carried out the detailed interaction analysis of lectins from various origins with *N*-linked glycans and amino acid residues of the SARS-CoV-2 S glycoproteins and results are summarized in Tables 3 and 4, respectively. The macromolecular docking suggests that the binding affinity (–269.31 kcal/mol) of NPA towards SARS-CoV-2 S glycoprotein was found maximum in all the lectins used in docking studies. Figure 3(a) illustrates that NPA interacted with *N*-linked glycans by forming similar H-bonding patterns like PRM-A. The NPA forms three H-bonds by Val94, Gly60 and Ile96 residues with FUC1320, MAN1324 and NAG1322, respectively. Aromatic H-bond interactions were also seen between Trp37, Tyr97 and NAG1321, BMA1323, respectively. Furthermore, the NPA forms residue-residue interactions with SARS- CoV-2 S glycoprotein. Figure 3(b) shows interactions of amino acids of NPA with residues of SARS-CoV-2 S glycoprotein and detailed interaction analysis is reported in Table 4.

In the case of GRFT, a single interaction was observed with SARS-CoV-2 S glycans. The H-bond formation by GRFT residue, i.e. Asp67 with MAN1325 at a bond distance of 2.20 Å is shown in Figure 3(c). Figure 3(d) shows the binding of GRFT with amino acid residues of SARS-CoV-2 S. The residues of GRFT like Thr51, Ala92 were involved in H-bonding with Thr236 and Pro527 of SARS-CoV-2 S. Also, Ser88 formed two H-bonds with SARS-CoV-2 S amino acids viz. Ser366 and Asn370 at bond distances of 2.10 Å and 1.76 Å, respectively. Figure 3(e) represents the docked complex of CV-N with SARS-CoV-2 S glycoprotein which gives −230.9 kcal/mol binding energy by forming one hydrogen bond with MAN1325. Similarly, CV-N forms residual bonding between amino acid Lys84 with Asn87 of SARS CoV-2 S glycoprotein at 2.63 Å bond distance Figure 3(f).

Potential clinical applicability of antiviral lectins is limited due to associated unfavorable responses such as mitogenicity, hemagglutination and inflammation (Balzarini, 2007a; Gupta et al., 2020). Therefore, we decided to perform the macromolecular docking of BanLec with SARS-CoV-2 S glycoprotein by using wild-type (PDB ID: 3MIT) as well as a mutant (H84T, in which the mitogenic activity of BanLec is separated from the antiviral activity) (PDB ID: 4PIT) of BanLec. Docked complexes of BanLec (wild-type and the mutant) with SARS-CoV-2 S glycoprotein, gave docking energy of −219.8 kcal/mol and −220.7 kcal/mol, respectively. In the molecular docking, the mutant (H84T) and the wild-type BanLec lectin showed variable interactions with the S glycoprotein glycans of SARS-CoV-2 (Table 3). Furthermore, the interactions between BanLec and S glycoprotein amino acids were also found to be different in both the docked complexes (wild-

Table 3. Detailed interaction analysis of lectins with *N*-linked glycans of SARS-CoV-2 spike glycoprotein.

Plant lectins	PDB ID	Docking energy (kcal/mol)	Interacting residues of Lectins	Interacted SARS CoV-2 S Glycans	Bond type	Bond distance (Å)
NPA	1NPL	−269.3	Val94	FUC1320	HB	2.56
			Try97	BMA1323	Ar-HB	2.68
			Gly60	MAN1324	HB	2.22
			Ile96	NAG1322	HB	2.19
			Trp73	NAG1321	Ar-HB	2.33
GRFT	2GUD	−252.3	Asp67	MAN1325	HB	2.20
CV-N	3GXZ	−230.9	Asp95	MAN1325	HB	1.33
BanLec	3MIT (*Wild-type*)	−219.8	Phe104	MAN1325	Ar-HB	1.99
	4PIT (*Mutant H84T*)	−220.7	Thr84	BMA1323	HB	1.60
			Lys130	MAN1325	HB	2.43
			Phe131	BMA1323	Ar-HB	2.01
UDA	1EHD	−190.5	Gln6	Man1324	HB	1.09
			Arg33	Man1325	HB	2.53
			Trp21	NAG1322	Ar-HB	2.24

Table 4. Detailed interaction analysis of lectins with amino acids of SARS CoV-2 spike glycoprotein.

Plant lectins	PDB ID	Docking energy (kcal/mol)	Interacting residues of lectin	Interacted SARS CoV-2 S amino acids	Bond type	Bond distance (Å)
NPA	1NPL	−269.3	Asn44	Thr345	HB	2.65
			Trp73	Asn343	HB	2.20
			Trp73	Asn343	Ar-HB	2.60
GRFT	2GUD	−252.3	Thr51	Thr236	HB	2.56
			Arg64	Asp364	Salt Bridge	4.77
			Ser88	Ser366	HB	2.10
			Ser88	Asn370	HB	1.76
			Ala92	Pro527	HB	2.77
CV-N	3GXZ	−230.9	Lys84	Asn87	HB	2.63
BanLec	3MIT (*Wild-type*)	−219.8	Lys6	Glu132	Salt Bridge	2.50
			Ala17	Asn234	HB	1.30
			Ala17	Gly232	HB	1.24
			Tyr83	Asn370	Ar-HB	2.78
	4PIT (*Mutant H84T*)	−220.7	Asp19	Lys529	Salt Bridge	2.48
			Tyr101	Arg237	Pi-cation	5.45
UDA	1EHD	−190.5	Trp21	Asn370	Ar-HB	1.90

type and mutant; Table 4). In the wild-type BanLec docked complex the amino acid Phe104 was the only one to interact with MAN1325 of S glycoprotein via aromatic hydrogen bond. The rest of the amino acids, i.e. Lys6 and Tyr83 of wild-type BanLec were seen to interact with Glu132 and Asn370 of S glycoprotein through the salt bridge and aromatic hydrogen bond, respectively, while Ala17 of wild-type BanLec was seen to interact with both Gly232 and Asn234 of S glycoprotein through hydrogen bonds (Figure 4(a,b)). The amino acids Asp19, Tyr101 of BanLec mutant were seen to interact with amino acids of S glycoprotein Lys529 and Arg237 individually through the salt bridge and pi-cation, respectively. Furthermore, the amino acid Phe131 of BanLec mutant interacted with BMA1323 S glycoprotein through an aromatic hydrogen bond, while the amino acid Lys130 of the BanLec mutant formed a hydrogen bond with the MAN1325 of the S glycoprotein. Surprisingly, the point of mutation, i.e. Thr84 in BanLec mutant was seen to with BMA1323 of the S glycoprotein via one hydrogen bond (Figure 4(c,d)). We also analyzed the interactions of UDA with the S glycoprotein and found good docking energy of −190.5 kcal/mol. The amino acids Gln6 and Arg33 of UDA were seen to interact with MAN1324 and MAN1325 via hydrogen bonds, respectively. While the amino acid Trp21 of UDA was seen to interact with both the NAG1322 and Asn370 of S glycoprotein via aromatic hydrogen bonds (Figure 5).

RMSDs of SARS-CoV-2 S glycoprotein with PRM-A and all the lectins

The conformational changes of S glycoprotein with PRM-A and all the lectins were compared with the initial docking complex pose. The RMSD analysis reveals that the S glycoprotein displayed high flexibility during the 100 ns MD simulation. Figure 6 illustrates that the average RMSD values for S glycoprotein for all 100 ns MD simulations. During the initial time period of PRM-A-S glycoprotein MD simulation the deviation in the S glycoprotein was not drastic and remained below 15 Å (light blue color). However, after 60 ns the RMSD value of the S glycoprotein raised to 15 Å and was stable around 15 Å for the remaining 40 ns. During the NPA-S glycoprotein, MD simulation the RMSD value for S glycoprotein during the simulation of NPA-S glycoprotein was observed to be between 14 Å and 16 Å from 20 ns (brown color). Surprisingly, in GRFT-S glycoprotein MD simulation the deviation in the RMSD value of S glycoprotein drastically deviated from 10 Å to 20 Å throughout the 100 ns MD simulation

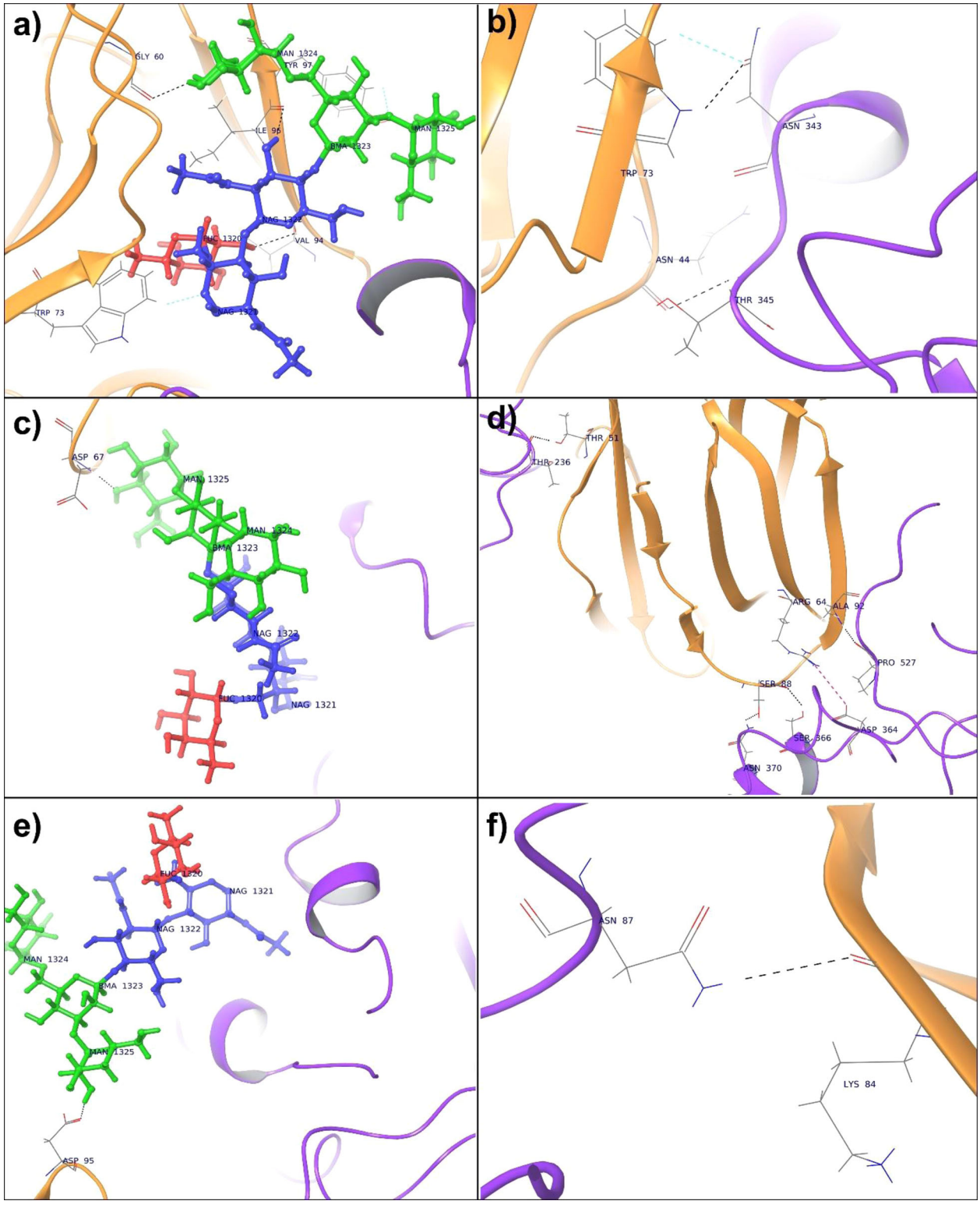

Figure 3. (a) Binding mode of NPA with *N*-linked glycans of SARS-CoV-2 spike glycoprotein. (b) Intermolecular interactions between NPA and SARS-CoV-2 spike glycoprotein. (c) Binding mode of GRFT with *N*-linked glycans of SARS-CoV-2 spike glycoprotein; (d) Intermolecular interactions between GRFT and SARS-CoV-2 spike glycoprotein. (e) Binding mode of CV-N with *N*-linked glycans of SARS-CoV-2 spike glycoprotein; (f) Intermolecular interactions between CV-N and SARS-CoV-2 spike glycoprotein.

(grey color). For CV-N- S glycoprotein 100 ns MD simulation very less deviation was observed in the S glycoprotein and post 15 ns the RMSD value remained between 20 Å and 15 Å (yellow color). For both BanLec wild-type - S glycoprotein 100 ns MD simulation (Blue, Accent 1 color) and BanLec mutant-S glycoprotein (green color) 100 ns MD simulation, the RMSD value of S glycoprotein did deviate a bit in the first 20 ns but remained below 15 Å. Surprisingly, post 25 ns, no drastic deviation was observed in the RMSD value of S glycoprotein for both the 100 ns MD simulations. The RMSD

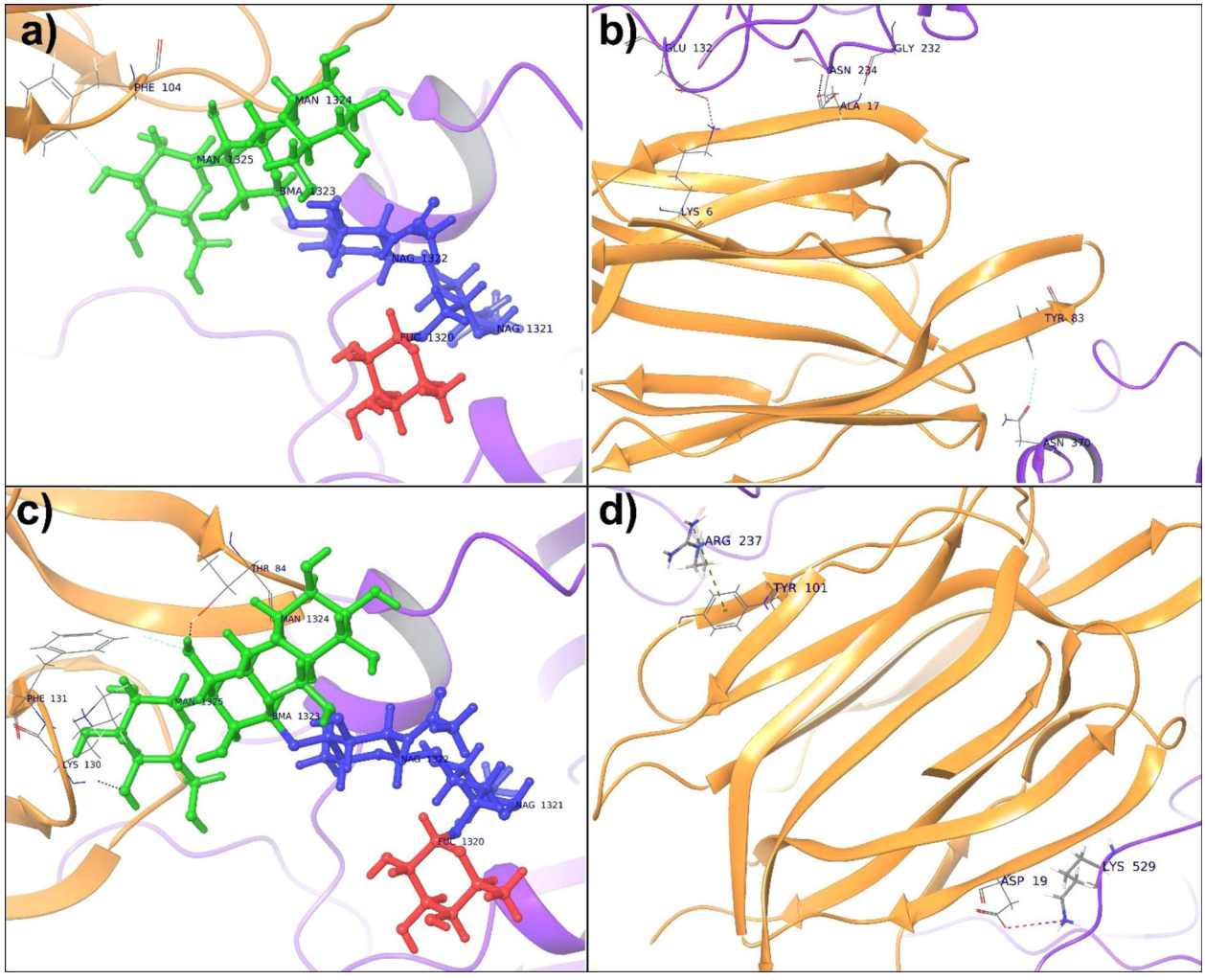

Figure 4. (a) Binding mode of wild-type BanLec with *N*-linked glycans of SARS-CoV-2 spike glycoprotein; (b) Intermolecular interactions between wild-type BanLec and SARS-CoV-2 spike glycoprotein. (c) Binding mode of mutant BanLec with *N*-linked glycans of SARS-CoV-2 spike glycoprotein; (d) Intermolecular interactions between mutant BanLec and SARS-CoV-2 spike glycoprotein.

value for S glycoprotein in UDA-S glycoprotein 100 ns MD simulation showed deviation in between 10 Å and 15 Å, while it declined to 10 Å from 60 ns to 70 ns and went above 15 Å during the final time period of 100 ns MD simulation (dark blue color). This flexibility and thermodynamic instability of S glycoprotein can be conferred on the presence of several loop regions in the RBD and NTD region of the crystal structure (PDB ID: 6WPS). The stability of the docked complexes of PRM-A-S glycoprotein and lectins-S glycoprotein were further investigated by the simulation event analysis and Root Mean Square Fluctuation (RMSF) (Supporting Information Figure S1). The intermolecular H-bonds formed between PRM-A-SARS-CoV-2 S glycoprotein, PRM-A-S glycoprotein glycans, lectins-SARS-CoV-2 S glycoprotein and lectins-S glycoprotein glycans were determined.

Simulation interaction analysis of PRM-A with S glycoprotein

During the 100 ns MD simulation less deviation of bound PRM-A at the binding site of S glycoprotein was observed (Figure 7). At about 63 ns an average RMSD of 2 Å was seen, while after 63 ns, slight conformational changes (averaged RMSD 3 Å) were found in the bound PRM-A, due to highly rotational bonds (single) in the PRM-A structure (light blue color). Low levels of RMSD value for PRM-A suggest stronger binding with the S glycoprotein. It was observed that the number of bonding interactions between PRM-A and SARS-CoV-2 S glycoprotein was constant during 80 ns (Figure 8). The interactions between PRM-A-S glycoprotein are mainly due to residues Asp364, Ser366, Val367, Asn370, Ser371 and Ser373 which intact the PRM-A tightly bound to the S glycoprotein. Conversely, PRM-A also binds with glycans very tightly up to the simulation time period of 80 ns (Figure 9). From the 100 ns MD simulation event analysis, we also observed that PRM-A underwent significant structural changes after 80 ns and it forms interactions with other amino acids like Asn437, Asn439 and Asn440 with changing its binding pose at RBD binding site. It seems interactions of PRM-A with glycans were found to be broken and to reduce the number of interactions after 80 ns (Figure 9). The simulation of PRM-A with the SARS-CoV-2 S glycoprotein displayed multiple bindings of PRM-A to the glycans and amino acids of S glycoprotein. In the simulation Video 1, initial binding phase of PRM-A with the S glycoprotein (up to 70 ns), initial interactions were observed between the disaccharide moiety of PRM-A and glycan of

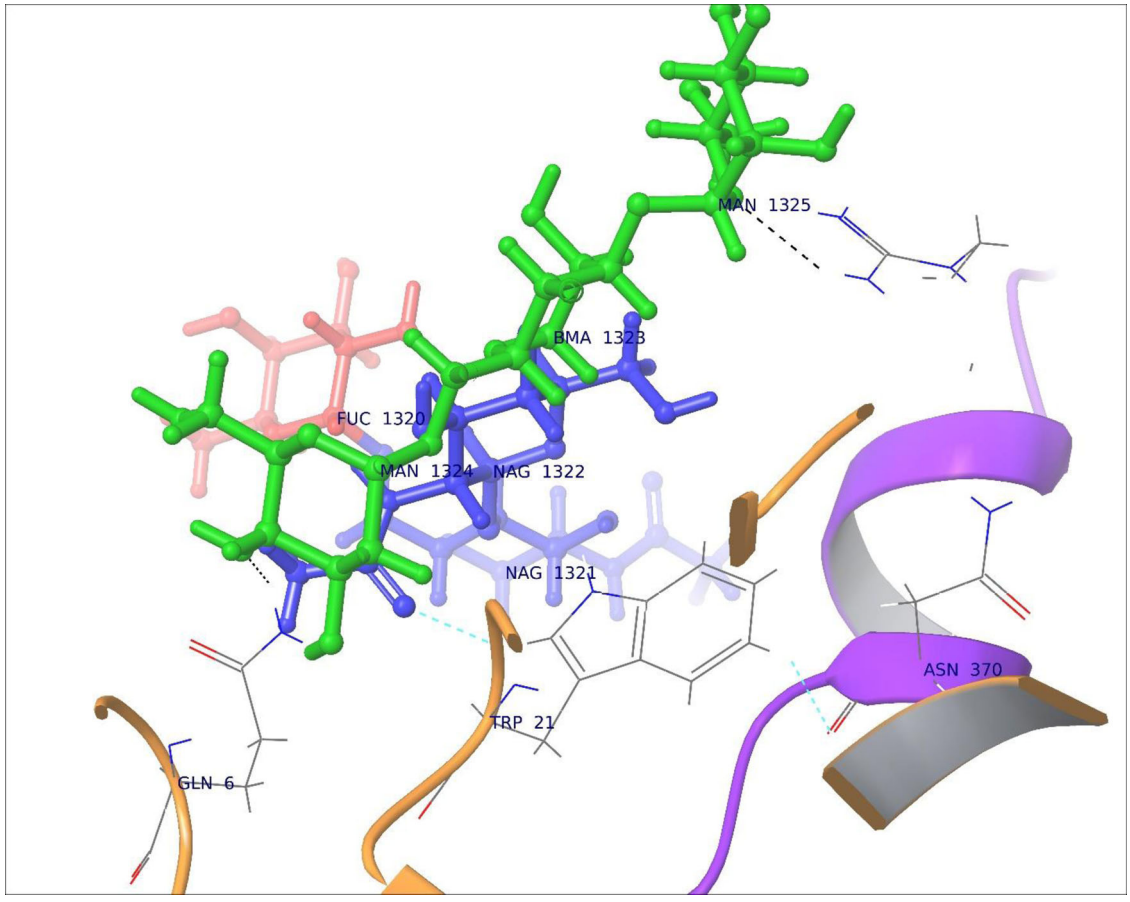

Figure 5. Binding mode of UDA with *N*-linked glycans and amino acids of SARS-CoV-2 spike glycoprotein.

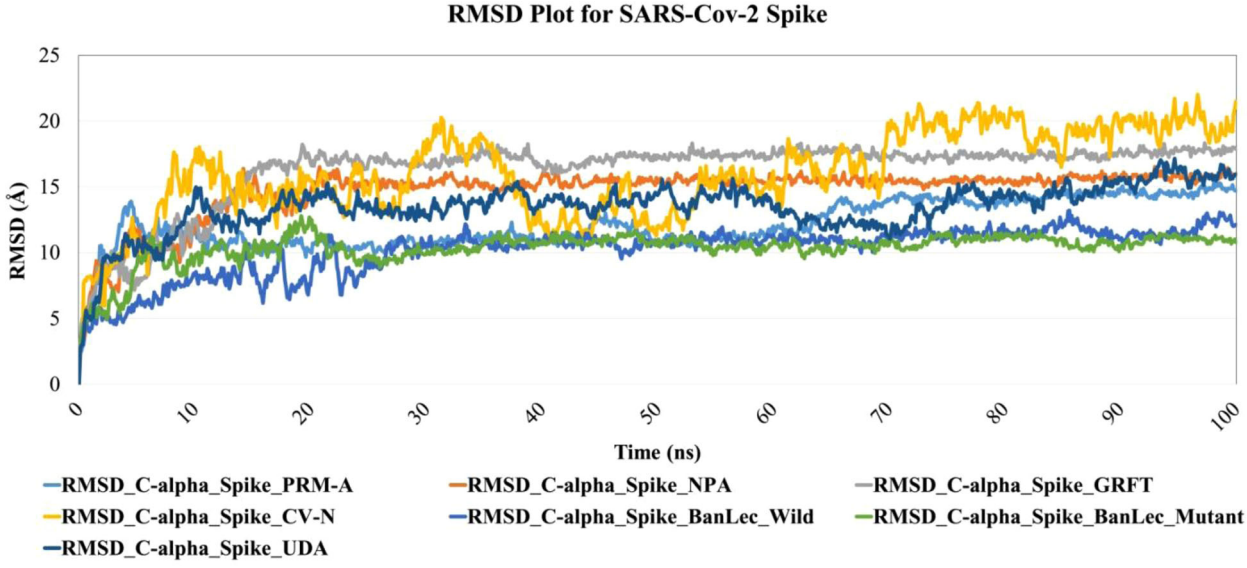

Figure 6. Time-dependent root mean square (RMSD) of S glycoprotein with PRM-A and all the lectins.

S glycoprotein. The five membered ring structure (ABCDE) was also seen to interact with the amino acids (Asp364, Ser366, Val367) and also with the glycans of S glycoprotein. Surprisingly, the D-Alanine moiety was seen to interact only with the glycan of S glycoprotein. During the time interval of 70 ns–80 ns, the PRM-A disassociated from S glycoprotein and a 180° conformational flip of the disaccharide moiety of PRM-A was observed (Figure 10). Post-flip, the D-Alanine moiety was seen to interact with the amino acids (Asn370, Ser371 and Ser373) of the S glycoprotein. During the final phase of simulation, the disaccharide moiety interacted with Asn437, Asn439 and Asn440 of the S glycoprotein.

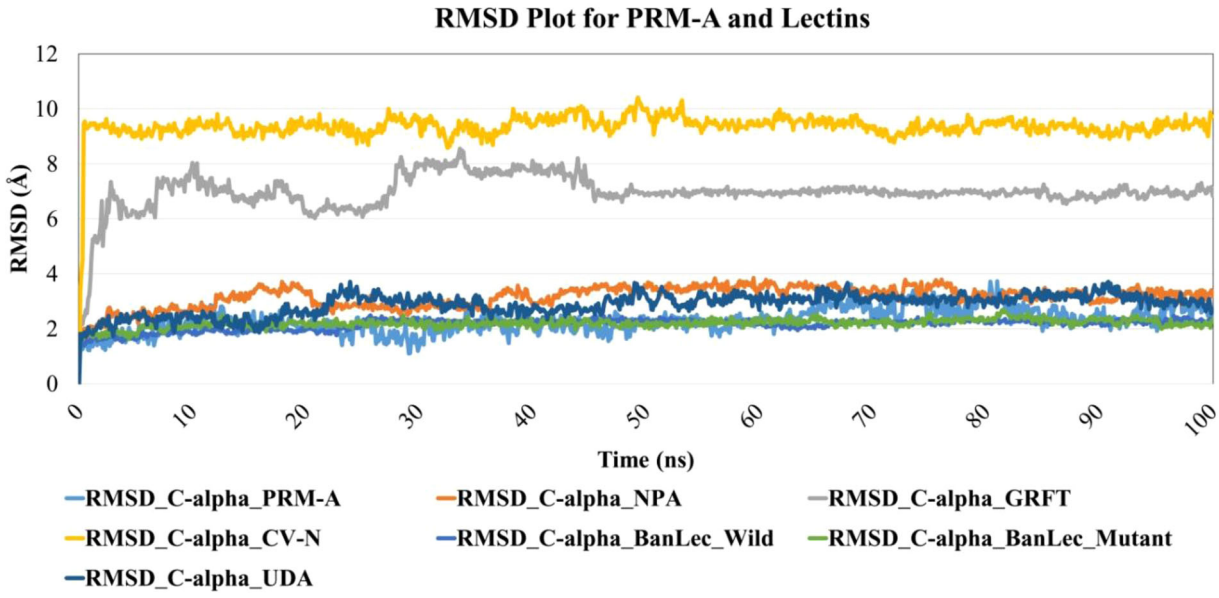

Figure 7. Time-dependent Root Mean Square (RMSD) PRM-A and lectins with SARS-CoV-2 S glycoprotein.

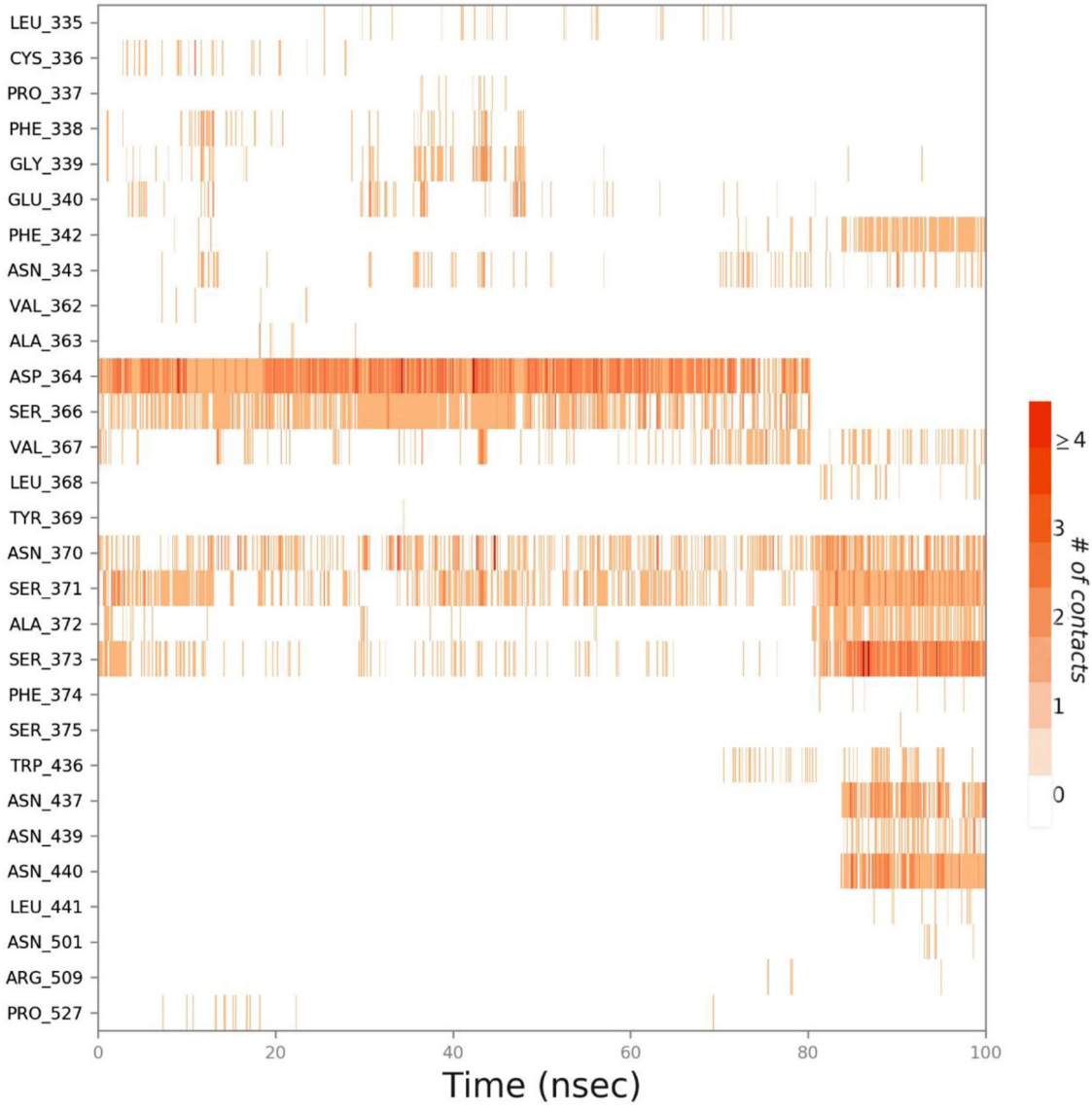

Figure 8. A time-dependent interactions occurring during the course of 100 ns MD simulation. The figure shows residual interaction with the PRM-A in each trajectory. Few amino acids form more than one specific interaction with the PRM-A, which is shown by a dark shade of orange, according to the scale of the plot.

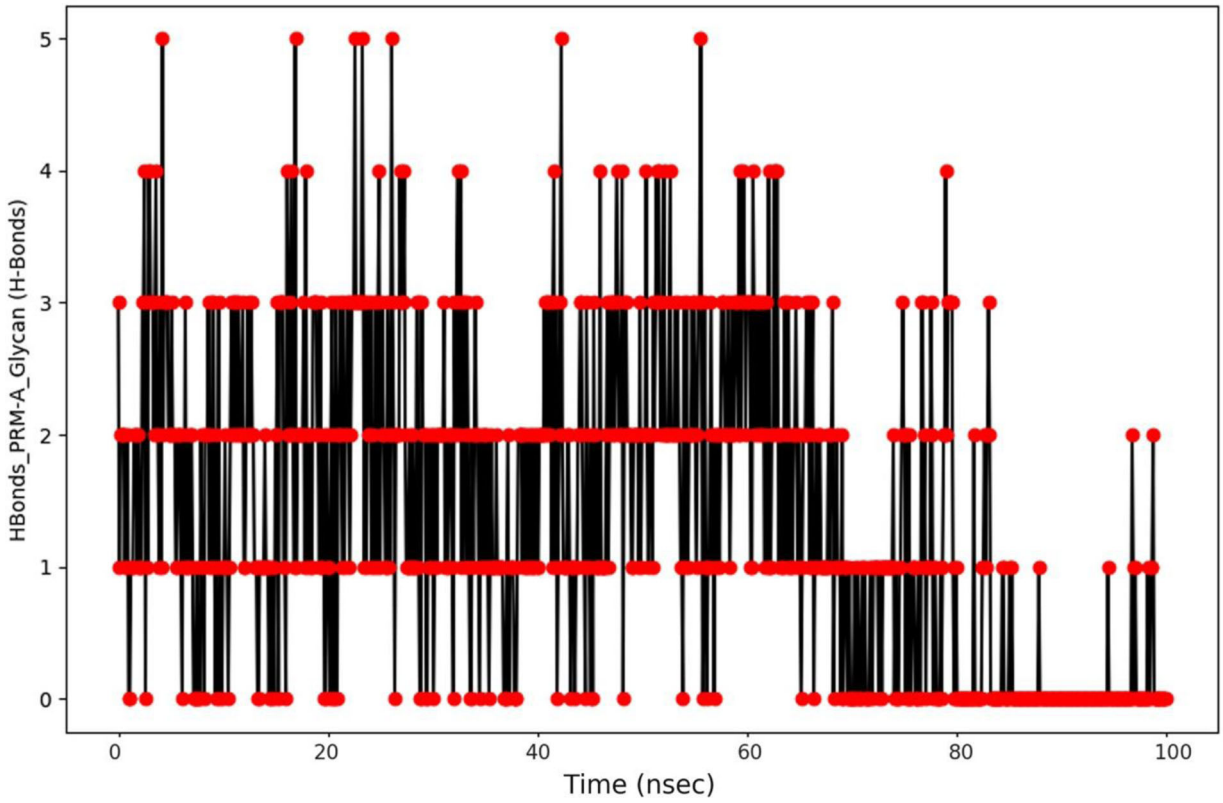

Figure 9. Hydrogen bond interactions between PRM-A and S glycoprotein glycans.

Simulation interaction analysis of NPA with S glycoprotein

The dynamic behavior of NPA was observed as it interacted well with both glycans and amino acids of the S glycoprotein. The interaction between NPA and S glycoprotein was stabilized from about 20 ns suggesting a strong interaction complex (Video 2). During the first 40 ns NPA was seen to interact more with the amino acids of S glycoprotein while only a few hydrogen bonds were observed between the glycans of S glycoprotein and NPA (Figure 11(a,b)). However, near about 60 ns about 14 hydrogen bonds are observed, and post 60 ns the lectin is seen to interact more with glycans of S glycoprotein. The amino acids Trp73 and Asn343 of NPA and S glycoprotein, respectively, were observed to interact through the 100 ns MD simulation. MAN1324, BMA1323, MAN1325, FUC1320 NAG1321 and NAG1322 of the S glycoprotein were seen to interact with the amino acids of NPA (Val94, Asn93, Phe23, Arg92, Ile96) suggesting that the lectin strongly interacted with the glycans of S glycoprotein. At various time points, the amino acids of NPA and S glycoprotein were seen to be in contact through various bonds like H-bond, Ar-H-bond, etc. The hydrogen bonding graph and the interaction analysis of NPA with S glycoprotein amino acids show a similar pattern wherein, the number of hydrogen bonds in the initial 40 ns is comparatively less, while a surge in the number of hydrogen bonds is observed at around 60 ns similarly to the interaction analysis. Post 60 ns, the number of hydrogen bonds is seen to decline in both the graph and interaction analysis.

Simulation interaction analysis of GRFT with S glycoprotein

The dynamic behavior of GRFT displayed variable RMSD value with the S glycoprotein (Figure 7) wherein the RMSD value deviated in the range of 6 Å to 8 Å during the first 50 ns. However, the RMSD value was stabilized after 50 ns as the number of hydrogen bonds remained near about the same in the second half of the 100 ns MD simulation. GRFT was seen to interact more with the amino acids of S glycoprotein wherein at about 20 ns near about 14 hydrogen bonds are formed. During the first 20 ns, the number of hydrogen bonds between GRFT and amino acids of S glycoprotein declined from 10 to 2. Surprisingly, very few hydrogen bonds are seen in between the glycans of S glycoprotein and GRFT. At about 10 ns to 15 ns, only a few hydrogen bonds were seen between the glycans of S glycoprotein and GRFT while, only 1 hydrogen bond was observed at about 20 ns after which no hydrogen bonds were observed between glycans of S glycoprotein and GRFT (Figure 12(a,b)). The amino acids Asp67 and Tyr68 of GRFT were the only ones to interact with the glycans MAN1325 and BMA1323 of the S glycoprotein, respectively. As previously mentioned no glycan-amino acid interaction was seen between GRFT and S glycoprotein from 30 ns to 100 ns. The amino acids Arg64 and Gln271 of GRFT were seen to interact with various amino acids of S glycoprotein for the initial 30 ns, while the amino acid Asp35 of GRFT was seen to interact mostly with Tyr28 of S glycoprotein during the 100 ns MD simulation. Surprisingly, Thr323 of S glycoprotein was

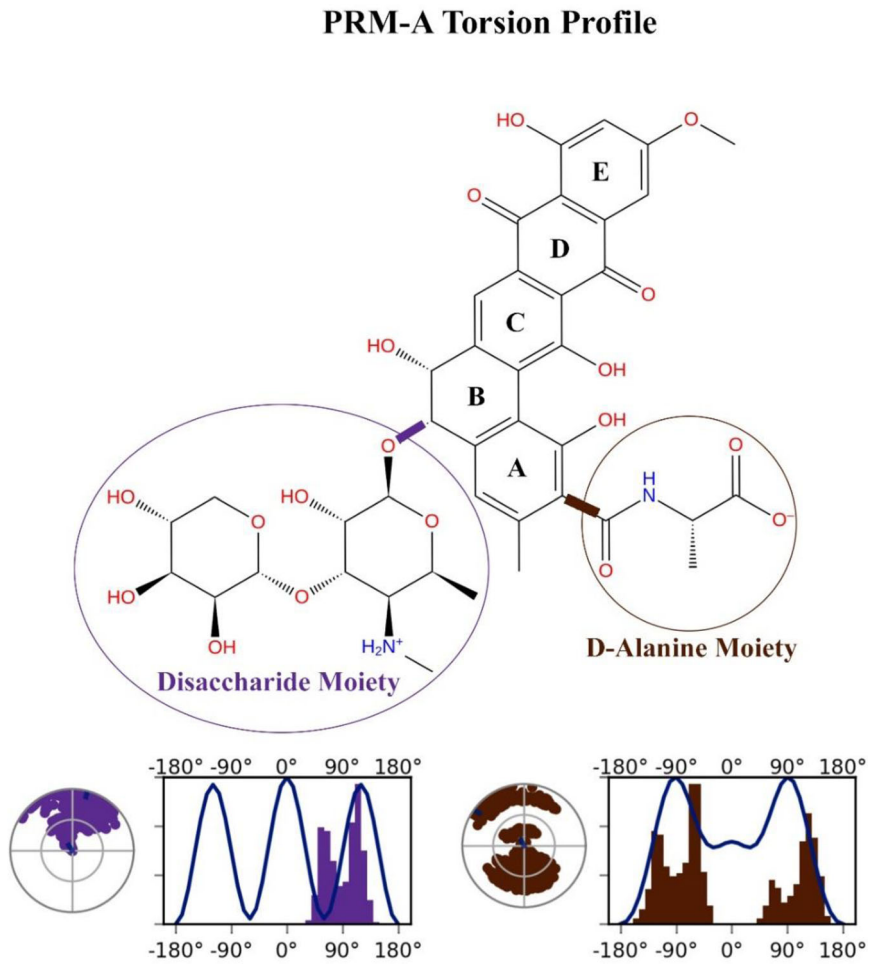

Figure 10. The PRM-A torsion profile elaborates on the conformational changes of the rotatable bond of ring A and ring B which attaches to the D-Alanine and Disaccharide moiety, respectively, the 100 ns simulation trajectory. The rotatable bond torsion is elucidated by a bar plot and a dial plot of similar color. Dial plots show the conformational variations of the torsion during the 100 ns MD simulation.

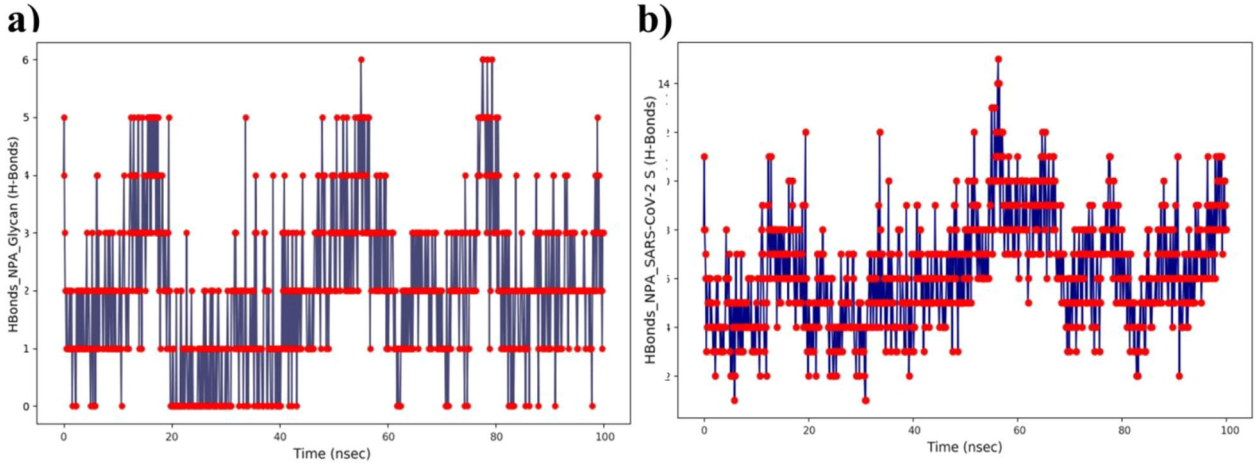

Figure 11. Hydrogen bonding between NPA and (a) Glycans of S glycoprotein (b) Amino acids of S glycoprotein.

seen to interact throughout the 100 ns MD simulation. Asn97 of GRFT was observed to interact with the Thr323 of S glycoprotein during 20 ns to 70 ns **(**Video 3**)**. The interaction analysis of hydrogen bonding between GRFT and S glycoprotein amino acids shows a similar pattern as observed in the hydrogen bonding graph (Figure 12(b)). During the initial phase of 100 ns MD simulation more hydrogen bond formation was observed in the interaction analysis and the hydrogen bonding graph of amino acids. Post 20 ns the number of hydrogen bonds was reduced in the hydrogen bonding graph which was also seen in the interaction analysis of the same.

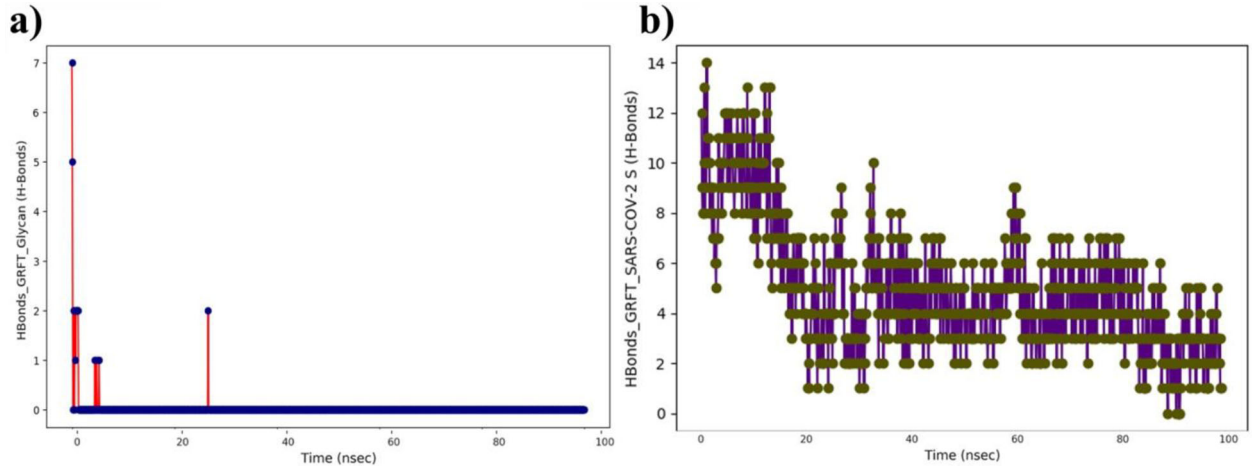

Figure 12. Hydrogen bonding between GRFT and (a) Glycans of S glycoprotein (b) Amino acids of S glycoprotein.

Simulation interaction analysis of CV-N with S glycoprotein

The dynamic behavior of CV-N was seen to be highest amongst the other lectins (i.e. ~10 Å; Figure 7), despite the multiple interactions with amino acids and glycan of S glycoprotein. The RMSD value remained between 10 Å and 8 Å throughout the 100 ns MD simulation. A similar deviation was observed in the RMSD value of S glycoprotein during the CV-N-S glycoprotein 100 ns MD simulation. CV-N lectin was seen to interact with amino acids and glycans of S glycoprotein throughout the 100 ns simulation. During the first 50 ns near about 4 to 8 hydrogen bonds were observed between S glycoprotein amino acids and CV-N while about 5 to 6 hydrogen bonds were seen in between glycans of S glycoprotein and CV-N. At about 60 ns more hydrogen bonds were seen in both glycans, amino acids of S glycoprotein and CV-N. Towards the end of 100 ns simulation CV-N was seen to interact more with the amino acids of S glycoprotein by forming near about 8 to 14 hydrogen bonds as compared to the formation of about 5 hydrogen bonds with the glycans of S glycoprotein (Figure 13(a,b)). The amino acid Asp95 of CV-N was seen to interact with MAN1325 of S glycoprotein at the initial phase and was also seen to interact with various amino acids of S glycoprotein throughout the 100 ns MD simulation run. The amino acids Gly96 and Asn93 from CV-N were seen to interact in the initial 30 ns of the 100 ns MD simulation. Ser66 and Thr618 of CV-N interacted with various amino acids of S glycoprotein from about 20 ns to 100 ns, while Asn26 was seen to interact in the latter half of the 100 ns MD simulation. Amino acids Glu68 and Gly65 of CV-N interacted with the amino acids of S glycoprotein from 80 ns to 100 ns only. Similarly, the amino acid Lys529 of S glycoprotein was seen to interact throughout the 100 ns MD simulation, while Ser325 and Ser530 interacted from 10 ns to 100 ns. Both the amino acids Glu654 and Asn641 were seen to interact in the latter half of the 100 ns MD simulation **(**Video 4**)**. The amino acids interaction analysis of CV-N with S glycoprotein amino acids displayed less number of hydrogen bonding in the initial phase of the 100 ns MD simulation. A similar pattern was also observed in the CV-N-S glycoprotein amino acid hydrogen bonding graph (Figure 13(b)). Post 50 ns increment in the number of amino acids was observed in both the amino acid interaction analysis and hydrogen bonding graph of CV-N with amino acids of S glycoprotein. During the last 30 ns of 100 ns MD simulation, the number of hydrogen bonds was stable in both the amino acid interaction analysis and hydrogen bonding graph of CV-N with amino acids of S glycoprotein.

Simulation interaction analysis of wild-type BanLec with S glycoprotein

The RMSD value for the BanLec wild-type lectin did not change throughout the 100 ns MD simulation and remained at 2 Å averaged. Despite the decline in the number of hydrogen bonds between 60 ns to 80 ns, the RMSD value remained at around 2 Å (Figure 7). This dynamic behavior of BanLec wild-type could be ascribed to the stable hydrogen bonding with both the glycans and amino acids of S glycoprotein. The wild-type BanLec was seen to form a maximum of 4 hydrogen bonds with the glycans of S glycoprotein throughout the 100 ns simulation. However, near about 75 ns to 80 ns, no hydrogen bonding was observed between glycans of S glycoprotein and wild-type BanLec. Surprisingly, the wild-type BanLec interacted more with the amino acids of S glycoprotein. On average near about 10 to 12 hydrogen bonds were observed throughout the 100 ns simulation. Till 60 ns, the numbers of hydrogen bonds were seen to increase with time after which there was a sudden drop in the number of hydrogen bonds till 70 ns, and in the last 30 ns 6 to 14 hydrogen bonds were observed between amino acids of S glycoprotein and wild-type BanLec (Figure 14(a,b)). The amino acids Glu79, Ala17 and Gly51 of wild-type BanLec were seen to interact throughout the 100 ns MD simulation. Glu79 of wild-type BanLec was seen to interact with BMA1323, MAN1324 and MAN1325 of the S glycoprotein, with more interactions with the MAN1325. His84 of wild-type BanLec also interacted well with the amino acids of S glycoprotein at various time intervals. Both the Gly108 and Gly109 were seen to interact from 20 ns to 100 ns with glycans and amino acids of S glycoprotein as well. Ser16 of wild-type BanLec was also seen to interact for 70 ns, i.e. from 20 ns to 30 ns and then from 60 ns to 100 ns with amino acids of S

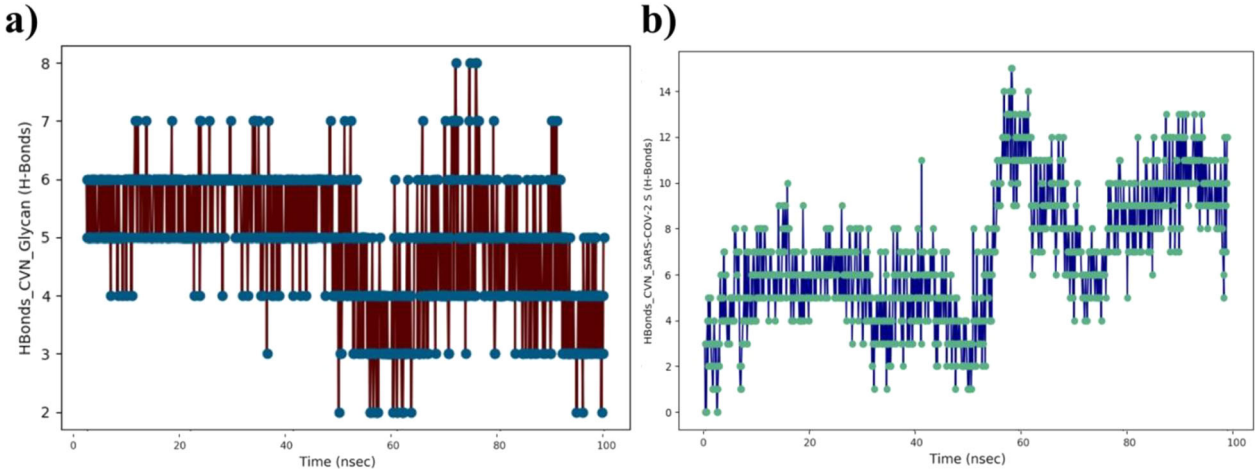

Figure 13. Hydrogen bonding between CV-N and (a) Glycans of S glycoprotein (b) Amino acids of S glycoprotein.

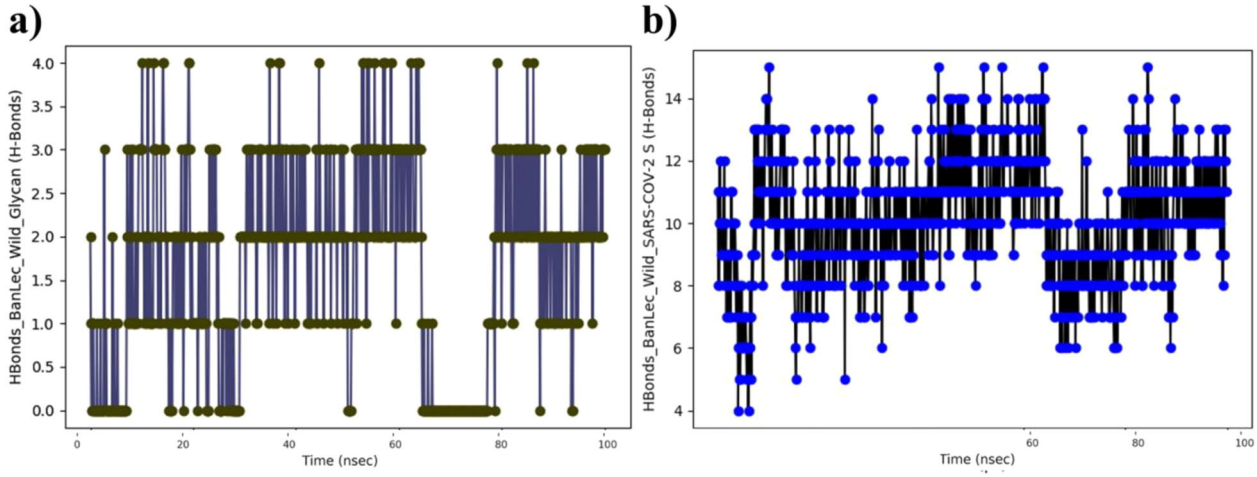

Figure 14. Hydrogen bonding between BanLec (wild-type) and (a) Glycans of S glycoprotein (b) Amino acids of S glycoprotein.

glycoprotein. The MAN1325, amino acids Asn370, Gly232, Asn234 and Arg237 of S glycoprotein were seen to interact constantly with the amino acids of wild-type BanLec. Tyr369 of S glycoprotein was seen to interact for about 90 ns, i.e. from 10 ns to 100 ns with the amino acids of wild-type BanLec **(**Video 5**)**. The interaction analysis of wild-type BanLec with both the glycans and amino acid of S glycoprotein displayed a similar pattern as observed in the hydrogen bonding graph (Figure 14(a,b)). The numbers of hydrogen bonds were observed to be the same on an average from 0 ns to 60 ns. A reduction in hydrogen bonds was observed between 60 ns and 70 ns in both the amino acid interaction analysis and hydrogen bond graph of S glycoprotein glycans (Figure 14(a)). However, post 70 ns the interactions remained similar for both the glycans and amino acids of S glycoprotein with wild-type BanLec.

Simulation interaction analysis of mutant BanLec with S glycoprotein

The RMSD value of mutant BanLec lectin did not change much and also remained at about 2 Å averaged as seen in BanLec wild-type throughout the 100 ns MD simulation (Figure 7). This suggests that single amino acid substitution did not affect the stability of the complex as compared to that of the wild-type complex. As compared to wild-type BanLec, the mutant BanLec was seen to form more hydrogen bonds with the glycans of S glycoprotein till 50 ns. However, after 50 ns the hydrogen bonding between glycans of S glycoprotein and mutant BanLec ranged from 0 to 4 till 100 ns. The mutant BanLec also interacted well with amino acids of S glycoprotein by forming hydrogen bonds ranging from 4 to 18 throughout the 100 ns simulation. During the first 20 ns the number of hydrogen bond varied from 5 to 15 while between 20 ns and 30 ns the bonding went up to 18 and then remained between 15 and 4 hydrogen bonds from 50 ns to 100 ns between the amino acids of S glycoprotein and mutant BanLec (Figure 15(a,b)). The single amino acid substitution in mutant BanLec (H84T), the amino acid Thr84 was seen to interact only in the initial 30 ns of the 100 ns MD simulation as compared to the His84 which was seen to interact with amino acids of S glycoprotein at various time points throughout the 100 ns MD simulation. The amino acid Arg127 was seen to interact with S glycoprotein throughout the 100 ns MD simulation. Furthermore, the amino acids Lys130, Phe131, Asp19 and Asp133 interacted with the S glycoprotein only in the first half of the 100 ns MD simulation. The amino acid Lys6 and Lys99 interacted with the S

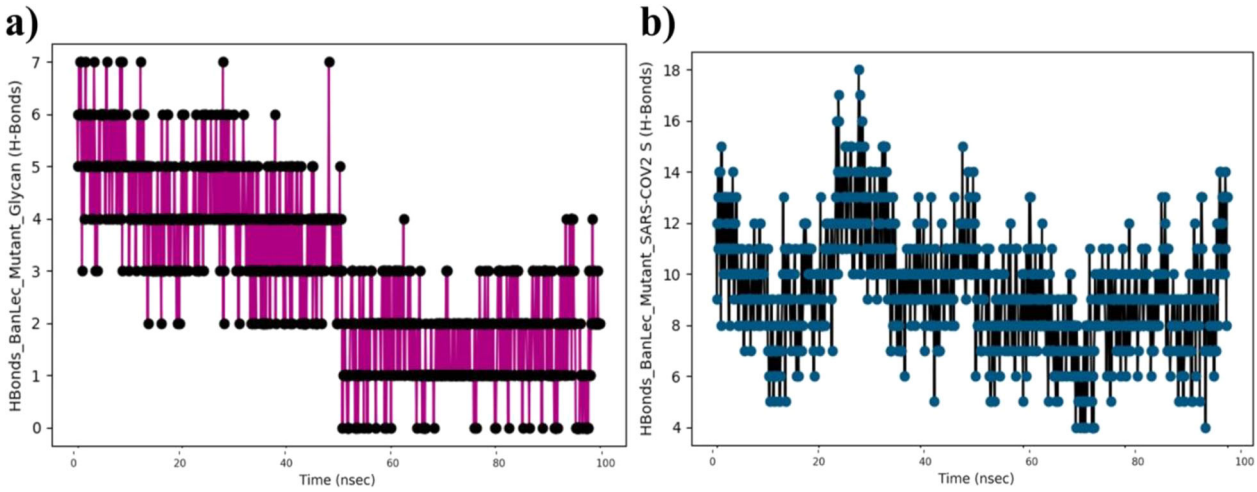

Figure 15. Hydrogen bonding between BanLec Mutant and (a) Glycans of S glycoprotein (b) Amino acids of S glycoprotein.

glycoprotein from 30 ns to 100 ns and from 20 ns to 100 ns, respectively. A couple of amino acids like Gly12 and Lys98 were seen to interact with the S glycoprotein during the second half of the 100 ns MD simulation. The glycans BMA1323, MAN1324 and MAN1325 were seen to interact well with the amino acids of mutant BanLec. Surprisingly, as similar to the observation in wild-type BanLec the MAN1325 of S glycoprotein was also seen to interact well with the amino acids of mutant BanLec. In the initial phase of the 100 ns MD simulation, the amino acid Arg237 of S glycoprotein was seen to interact well with the amino acids of mutant BanLec. Amino acids like Lys529, Asp364, Asp80 and Val83 of S glycoprotein displayed multiple interactions with the mutant BanLec throughout the 100 ns MD simulation. S glycoprotein amino acid Val83 interacted with the amino acids of mutant BanLec during the latter half of the 100 ns MD simulation **(**Video 6**)**. As compared to the hydrogen bonding graph of BanLec mutant-S glycoprotein (Figure 15(a)), a similar pattern was observed in the interaction analysis, wherein, the mutant BanLec interacted with multiple glycans during the first half of the 100 ns MD simulation. However, post 50 ns, the number of interactions of mutant BanLec with glycans of S glycoprotein was less. Surprisingly, the amino acid interaction analysis of mutant BanLec with amino acids of S glycoprotein displayed constant binding as seen in the hydrogen bonding graph (Figure 15(b)).

Simulation interaction analysis of UDA with S glycoprotein

During the first 20 ns, the RMSD value of UDA was not seen to deviate much and remained near 2 Å. However, after 20 ns visible deviation was observed between 4 Å and 2 Å for the rest 80 ns (Figure 7**)**. A small decline was seen in the RMSD curve of UDA at around 40 ns, which could be ascribed to the slight increase in the hydrogen bonding between UDA and amino acids of the S glycoprotein. UDA formed a stale complex by interacting with both the glycans and amino acids of S glycoprotein throughout the 100 ns MD simulation. The number of hydrogen bonds formed between glycans of S glycoprotein and UDA remained in the range of 2 to 4 throughout the simulation. However, till the initial 30 ns the hydrogen bonding between S glycoprotein amino acids and UDA remained in the range of 2–12, it went up to 16 and then gradually declined to 10 hydrogen bonds for the rest of the simulation time (Figure 16(a,b)). In the 100 ns MD simulation of UDA-S glycoprotein, the amino acids Arg33 and Gly36 of UDA were seen to interact with the MAN1324 and MAN1325, respectively, in the first 20 ns. Furthermore, Trp21 of UDA was seen to interact with the NAG1322 of S glycoprotein. In the second half of the 100 ns MD simulation no S glycoprotein glycan- UDA amino acid interaction was observed. Furthermore, Ser45 and Gly72 of UDA interacted with the amino acids of S glycoprotein at various time points throughout the 100 ns MD simulation. Surprisingly, PCA1 of UDA was also seen to interact with the S glycoprotein amino acid. In the second half of the 100 ns MD simulation, the amino acid Asp46 was seen at multiple time points. Trp69, Ser88, Ser89 of UDA were also seen to interact at various time points throughout the 100 ns MD simulation. Surprisingly, the glycans of S glycoprotein (MAN1324, MAN1325 and NAG1322) were seen to interact only in the first 40 ns of the MD simulation. Ile231 of the S glycoprotein was observed to interact throughout the 100 ns MD simulation study. The S glycoprotein amino acids like Glu132, Phe168, Gly232, Ala372 and Arg995 interacted with the amino acids of UDA at various time points throughout the 100 ns MD simulation. As observed in the H-bonding graph at 40 ns between amino acids of UDA and S glycoprotein (Figure 16(b)), a similar surge is observed, wherein about 10 H-bonds are observed at 40 ns. Post 40 ns, a declining interaction pattern is seen in the hydrogen bonding graph (Figure 16(b)), which was also observed in the interaction analysis of amino acids of UDA and amino acids of S glycoprotein **(**Video 7**)**.

Prime MM/GBSA binding free energies

MM/GBSA is known to be the best procedure for free binding energies (ΔG Bind) calculations in terms of hydrophobicity, VDW or solvation components. The screened molecules (PRM-A and all the lectins), serving as ligands to SARS-CoV-

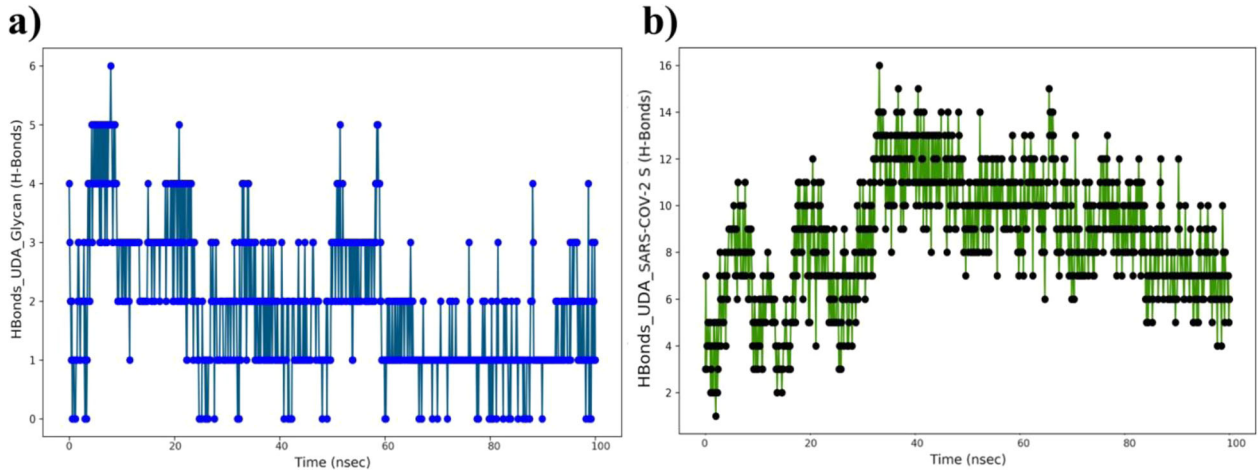

Figure 16. Hydrogen bonding between UDA and (a) Glycans of S glycoprotein (b) Amino acids of S glycoprotein.

Table 5. The ensemble-averaged Prime binding free energies (kcal/mol) of docked complexes during the 100 ns MD simulation.

Lead compounds complexed with SARS-CoV-2 S glycoprotein	ΔG bind[a] (kcal/mol)
PRM-A	−48.5 ± 0.7
NPA	−79 ± 1.3
GRFT	−73.7 ± 3.6
CV-N	−67.3 ± 3.1
BanLec Wild	−105.9 ± 3.1
BanLec Mutant	−115.4 ± 2.3
UDA	−98.3 ± 3.1

[a]ΔG Bind=MM/GBSA binding free energy.

2 S glycoprotein were submitted to ensemble-averaged Prime MM/GBSA method for a 100 ns MD simulation.

The ensemble-averaged MM/GBSA calculations of binding free energies of all the complexes are reported in Table 5. The protein–ligand complex is stronger when the binding energy is less (more negative value) (Lokhande et al., 2020). The data denotes that the BanLec mutant has the most negative binding free energy (−115.4 ± 2.3 kcal/mol) followed by BanLec wild-type (−105.9 ± 3.1 kcal/mol) which confers the binding stability of the BanLec mutant to be more potent followed by the BanLec wild-type lectin (Supporting Information Figure S2). Surprisingly, despite the lowest docking energy (−190.5 kcal/mol) the biding free energy of UDA (−98.3 ± 3.1 kcal/mol) also suggesting a strong complex. Despite their great docking scores the binding free energies of NPA, GRFT and CV-N were comparatively less than other lectins with binding energies about −79.016 ± 1.329 kcal/mol, −73.7 ± 3.6 kcal/mol and −67.3 ± 3.1 kcal/mol, respectively. The lectin mimic, PRM-A also showed favorable binding free energy with SARS-CoV-2 S glycoprotein with the binding free energy of about −48.5 ± 0.7 kcal/mol, suggesting that it also makes a strong complex with the SARS-CoV-2 S glycoprotein. These MM/GBSA results suggest that the lead molecules satisfy the Prime MM/GBSA approach to achieve a stable complex with SARS-CoV-2 S glycoprotein and all the energies predicted from the Prime MM/GBSA are thermodynamically favorable.

Discussion

As the S glycoprotein of SARS-CoV-2 is having 22 *N*-linked glycosylation sites occupied with complex and oligomannose type of glycans (Watanabe et al., 2020; Zhou et al., 2020), these glycans pose as interesting targets for targeted and novel antiviral development. However, understanding this glycan language is lagging behind the proteins due to its complex nature and existence of various conformations. In recent times, a key biological route of information transfer is considered via the sugar code which mediates cell–cell interactions and further signal transduction phenomenon. Lectins, which are carbohydrate-binding proteins, are considered as the decoder of this glycan information (sugar code) and are also considered the best fit for glycan recognition due to their structure and topological presentation. Indeed, this code-decode system is nowadays considered as the new storage system of biological information. By recognizing these glycans, lectins are employed in various biological processes like adhesion and growth regulation, cellular and immune responses (Gabius et al., 2011; Murphy et al., 2013). Due to their wide availability in nature and considerable use in several aspects of glycobiological research including potential antiviral agents against enveloped viruses (Botos et al., 2002; Keyaerts et al., 2007; van der Meer, de Haan, Schuurman, Haijema, Peumans, et al., 2007; van der Meer, de Haan, Schuurman, Haijema, Verheije, et al., 2007), these fascinating class of molecules (CBAs) have the potential to be repurposed as antivirals against SARS-CoV-2.

In general, CBAs specifically binds to the mannose residues of the *N*-linked glycans of glycoproteins present on the surface of the enveloped viruses, can block viral attachment and/or fusion to host cells (Balzarini, 2007b, 2007a). Recently, *Dolichos labalab* lectin I (DLL-I) has been reported to show anti-SARS-CoV-2 activity against n hCoV-19/Taiwan/NTU04/2020 strain with visible cytopathic effect. The binding study of DLL-I with recombinant S glycoprotein displays strong affinity and interaction with complex type *N*-glycans as compared to high-Mannose type *N*-glycans. This new report and previous studies of lectins from various sources against CoVs strengthen their potential to be used as antivirals (Liu et al., 2020). A recent docking analysis and simulation study predicted the probable binding site of the ACE2 receptor with the RBD of S glycoprotein wherein the Asn343 lies in close proximity of the predicted intermolecular glycan-glycan interactions between Asn74,

Asn165 of S glycoprotein and Ans546 of ACE2 receptor. Surprisingly, the Asn90 of ACE2 receptor was seen to interact at multiple sites of the S glycoprotein, while another glycan Asn322 of ACE2 was seen to interact to other regions of S glycoprotein (Zhao et al., 2020). Recently (Lenza et al., 2020) studied interactions of human galectins, Siglecs and C-type lectin receptors (CLRs) with the glycans present on the RBD (i.e. Asn331 and Asn343) wherein they found significant interactions between the glycans of the RBD of S glycoprotein and galectins, Siglecs and CLRs. Through MD simulation they also confirmed that the complexes which involved the presence of glycans of Asn343 displayed stronger and a vast number of interactions suggesting that the site Asn343 could be of great importance. The group also reported that the Galectin-3 and Galectin-8 interacted well with the glycans of S glycoprotein RBD while more information is required for Galectin-7. Siglec-8 did not recognize the glycans of S glycoprotein RBD, while Siglec-10 interacted well with the glycans. Furthermore, the CLRs (MGL and DC-SIGN) are also shown to interact with the glycans of S glycoprotein RBD. Therefore, targeting the glycosylation sites like Asn343, sites present in the RBD and other important sites could potentially inhibit the entry of the virus into the host cells. Since the CBAs have been widely used as antivirals against enveloped viruses including coronaviruses, we decided to study the binding of CBAs with glycans of S glycoproteins of SARS-CoV-2. Targeting CBAs towards the *N*-linked glycans of S glycoprotein could provide a new alternative for therapeutics in this current time of the pandemic. As reported earlier, the mannose binding lectins NPA, GRFT, CV-N, BanLec and GlcNAc binding lectin UDA have shown anti-viral properties against various enveloped viruses (Balzarini, 2007a; Botos et al., 2002; Covés-Datson et al., 2020; Mitchell et al., 2017; Rostock et al., 2005). As the envelope of these viruses and SARS-CoV-2 are covered with *N*-linked glycans we tried to study the interaction of all the lectins with the S glycoprotein of SARS-CoV-2 using docking and MD simulation and found that all the lectins interacted well with the glycans and also with the amino acids of S glycoprotein. Besides, our docking and MD simulation results also suggest that the binding of lectin-like non-peptidic mimic PRM-A occurred only with SARS-CoV-2 glycans without forming any bond with the protein.

In general, all the CBAs are proteinaceous except lectin-like non-peptidic mimic PRM-A, therefore, it is expected that all the CBAs will possess unfavorable responses such as immunogenicity, mitogenicity, hemagglutination and inflammatory activity. Therefore, redesigning CBAs using bioinformatics tools and at the same time retaining their broad-spectrum antiviral activity is an attractive strategy to consider. Taking this approach, we took the example of BanLec, where Swanson et al. (2015) showed that antiviral and mitogenic activities of a lectin can be separated via mutagenesis, and simultaneously, the resultant lectin maintains its broad-range antiviral activity. Single amino acid substitution in wild-type BanLec, where replacement of histidine with threonine at 84th position (H84T) in BanLec abolishes its mitogenic activity and significantly retained its broad-range antiviral activity. Indeed, specific amino-acid substitution retains its wild-type features and monovalent interactions. Furthermore, its broad-range antiviral activity was preserved by forming unique contacts involving the Thr84 side chain. We decided to compare the wild-type as well as a mutant of BanLec interaction with glycans of SARS-CoV-2. The docked complexes and MD simulation analyses of BanLec (wild-type and mutant type) showed similar docking energy and surprisingly the point of mutation, i.e. H84T of BanLec was seen to interact with SARS-CoV-2 S glycoprotein in both the complexes. In our study, we have also found that BanLec mutant has the most negative binding free energy (–115.4 ± 2.3 kcal/mol) followed by BanLec wild-type (–105.9 ± 3.1 kcal/mol) which confers the binding stability of the BanLec mutant to be more potent followed by the BanLec wild-type lectin to SARS-CoV-2 S glycoprotein. Surprisingly, the point of mutation (H84T) was also seen to interact well with the S glycoprotein of SARS-CoV-2 in both the wild-type and mutant BanLec suggesting that the single amino acid substitution did not affect the binding property of BanLec. These results also confirmed and suggest that all the lectins considered in our study can be engineered to remove the associated unfavorable responses using bioinformatics approaches and basic molecular biology techniques and can be tested for their neutralization property against SARS-CoV-2 and can emerge as novel antiviral therapy.

PRM-A which is composed of a disaccharide moiety linked to a 5,6-dihydrobenzo-α-naphthacenequinone substituted with D-alanine is a class of broad-spectrum fungicidal agents along with the antiviral activity. The antifungal activity of PRM-A ascribed to its rapid binding to yeast mannan in a Ca^{2+} dependent manner. The antiviral activity of PRM-A also depends upon binding to terminal mannose residue and Ca^{2+} to yield a ternary complex. Similarly, binding of gp120 with PRM-A was also found to be dependent upon the presence of Ca^{2+} in the buffer and the rate of dissociation of PRM-A from gp120 was significantly higher. Indeed, PRM-A was also found to be devoid of any immunological response. PRM-A is known to destabilize the membrane potential but no specific mechanism is known to show how PRM-A moves from cell wall to cell membrane (Balzarini et al., 2007; Nakagawa et al., 2013; Sawada et al., 1990). Based on the association-disassociation of PRM-A as suggested by the binding affinities and by MD simulation in our study, one can hypothesize an association-disassociation mechanism through which the PRM-A can move towards the cell membrane and can impart its activity. To understand the complete mechanism of PRM-A activity, further studies are warranted.

Therefore, using this simple basic bioengineering principle, it is possible to redesign these lectins, and uncoupling one activity from others may bring this broad spectrum CBAs into the clinic. In addition to that lectin-like small non-peptidic mimics should also be tested for their antiviral activity.

Conclusion

In conclusion, our study reports for the first time, the interaction of CBAs (lectins and lectin-like non-peptidic mimic PRM-A) with glycans of S glycoprotein of SARS-CoV-2 using molecular docking and MD simulation studies. In our study,

we have found that BanLec wild-type and its mutant form showed thermodynamically more stable binding complexes with SARS-CoV-2 S Glycoprotein. Our interaction studies of BanLec and its stable mutant form with glycans of S glycoprotein of SARS-CoV-2 also confirmed that using simple bioengineering principles it is possible to bring the broad-spectrum antiviral CBAs into the clinic. Additionally, PRM-A is another possible small lectin non-peptidic mimic that has the potential of being used as an antiviral against the SARS-CoV-2. Further, it would be interesting to test these CBAs against SARS-CoV-2 for their potential utilization as antiviral agents in the time of COVID-19 pandemic.

Acknowledgements

Authors acknowledge the Department of Science and Technology-Science and Engineering Research Board (DST-SERB), Govt. of India, New Delhi, (File Number: YSS/2015/002035) for Optimized Supercomputer facility for dynamics calculations. Authors thanks Mr. Krunal A. Mate, System Administrator, Dr. D. Y. Patil Vidyapeeth, Tathawade Campus for his prompt help in solving the technical problem during this study.

Disclosure statement

No potential conflict of interest was reported by the authors.

Funding

This work was supported by the Department of Science and Technology-Science and Engineering Research Board (DST-SERB), Government of India under the ECRA scheme [grant number ECR/2016/001187] and by Dr. D.Y. Patil Vidyapeeth, Pune [grant numbers DPU/106/18/2015, DPU/17/2016 (to Dr. Rajesh Kumar Gupta)]. Kiran Bharat Lokhande acknowledges the Indian Council of Medical Research (ICMR), New Delhi, for Senior Research Fellowship (Project ID: 2019-3458; file: ISRM/11(54)/2019).

References

Balzarini, J. (2007a). Carbohydrate-binding agents: A potential future cornerstone for the chemotherapy of enveloped viruses? *Antiviral Chemistry & Chemotherapy*, *18*(1), 1–11. https://doi.org/10.1177/095632020701800101

Balzarini, J. (2007b). Targeting the glycans of glycoproteins: A novel paradigm for antiviral therapy. *Nature Reviews. Microbiology*, *5*(8), 583–597. https://doi.org/10.1038/nrmicro1707

Balzarini, J., Van Laethem, K., Daelemans, D., Hatse, S., Bugatti, A., Rusnati, M., Igarashi, Y., Oki, T., & Schols, D. (2007). Pradimicin A, a carbohydrate-binding nonpeptidic lead compound for treatment of infections with viruses with highly glycosylated envelopes, such as human immunodeficiency virus. *Journal of Virology*, *81*(1), 362–373. https://doi.org/10.1128/JVI.01404-06

Berman, H. M., Westbrook, J., Feng, Z., Gilliland, G., Bhat, T. N., Weissig, H., Shindyalov, I. N., & Bourne, P. E. (2000). The Protein Data Bank/Biopython. *Nucleic Acids Research*, *28*(1), 235–242. https://doi.org/10.1093/nar/28.1.235

Bhardwaj, V. K., & Purohit, R. (2020a). Targeting the protein-protein interface pocket of Aurora-A-TPX2 complex: Rational drug design and validation. *Journal of Biomolecular Structure and Dynamics*, 1–10. Advance online publication. https://doi.org/10.1080/07391102.2020.1772109

Bhardwaj, V. K, & Purohit, R. (2020b). Computational investigation on effect of mutations in PCNA resulting in structural perturbations and inhibition of mismatch repair pathway. *Journal of Biomolecular Structure & Dynamics*, *38*(7), 1963–1974. https://doi.org/10.1080/07391102.2019.1621210

Bhardwaj, V. K., Singh, R., Sharma, J., Rajendran, V., Purohit, R., & Kumar, S. (2020). Identification of bioactive molecules from tea plant as SARS-CoV-2 main protease inhibitors. *Journal of Biomolecular Structure & Dynamics*, 1–10. Advance online publication. https://doi.org/10.1080/07391102.2020.1766572

Botos, I., O'Keefe, B. R., Shenoy, S. R., Cartner, L. K., Ratner, D. M., Seeberger, P. H., Boyd, M. R., & Wlodawer, A. (2002). Structures of the complexes of a potent anti-HIV protein cyanovirin-N and high mannose oligosaccharides. *The Journal of Biological Chemistry*, *277*(37), 34336–34342. https://doi.org/10.1074/jbc.M205909200

Bursulaya, B. D., Totrov, M., Abagyan, R., & Brooks, C. L. (2003). Comparative study of several algorithms for flexible ligand docking. *Journal of Computer-Aided Molecular Design*, *17*(11), 755–763. https://doi.org/10.1023/B:JCAM.0000017496.76572.6f

Covés-Datson, E. M., King, S. R., Legendre, M., Gupta, A., Chan, S. M., Gitlin, E., Kulkarni, V. V., Pantaleón García, J., Smee, D. F., Lipka, E., Evans, S. E., Tarbet, E. B., Ono, A., & Markovitz, D. M. (2020). A molecularly engineered antiviral banana lectin inhibits fusion and is efficacious against influenza virus infection in vivo. *Proceedings of the National Academy of Sciences of the United States of America*, *117*(4), 2122–2132. https://doi.org/10.1073/pnas.1915152117

Gabius, H.-J., André, S., Jiménez-Barbero, J., Romero, A., & Solís, D. (2011). From lectin structure to functional glycomics: Principles of the sugar code. *Trends in Biochemical Sciences*, *36*(6), 298–313. https://doi.org/10.1016/j.tibs.2011.01.005

Gupta, R. K., Apte, G. R., Lokhande, K. B., Mishra, S., & Pal, J. K. (2020). Carbohydrate-binding agents: Potential of repurposing for COVID-19 therapy. *Current Protein & Peptide Science*, *21*. Advance online publication. https://doi.org/10.2174/1389203721666200918153717

Harata, K., & Muraki, M. (2000). Crystal structures of Urtica dioica agglutinin and its complex with tri-N-acetylchitotriose. *Journal of Molecular Biology*, *297*(3), 673–681. https://doi.org/10.1006/jmbi.2000.3594

Keyaerts, E., Vijgen, L., Pannecouque, C., Van Damme, E., Peumans, W., Egberink, H., Balzarini, J., & Van Ranst, M. (2007). Plant lectins are potent inhibitors of coronaviruses by interfering with two targets in the viral replication cycle. *Antiviral Research*, *75*(3), 179–187. https://doi.org/10.1016/j.antiviral.2007.03.003

Kim, S., Chen, J., Cheng, T., Gindulyte, A., He, J., He, S., Li, Q., Shoemaker, B. A., Thiessen, P. A., Yu, B., Zaslavsky, L., Zhang, J., & Bolton, E. E. (2019). PubChem 2019 update: Improved access to chemical data. *Nucleic Acids Research*, *47*(D1), D1102–D1109. https://doi.org/10.1093/nar/gky1033

Lenza, M. P., Oyenarte, I., Diercks, T., Quintana, J. I., Gimeno, A., Bosch, A., Valle, M., Millet, O., Abrescia, N. G. A., Palazón, A., Marcelo, F., Jiménez-Osés, G., Jiménez-Barbero, J., Ardá, A., & Ereño-Orbea, J. (2020). Structural characterization of the N-linked glycans in the receptor binding domain of the SARS-CoV-2 spike protein and their interactions with human lectins using NMR spectroscopy. *Angewandte Chemie (International Ed. in English)*. Advance online publication. https://doi.org/10.1002/anie.202011015

Liu, Y.-M., Shahed-Al-Mahmud, M., Chen, X., Chen, T.-H., Liao, K.-S., Lo, J. M., Wu, Y.-M., Ho, M.-C., Wu, C.-Y., Wong, C.-H., Jan, J.-T., & Ma, C. (2020). A carbohydrate-binding protein from the edible lablab beans effectively blocks the infections of influenza viruses and SARS-CoV-2. *Cell Reports*, *32*(6), 108016. https://doi.org/10.1016/j.celrep.2020.108016

Lokhande, K. B., Doiphode, S., Vyas, R., & Swamy, K. V. (2020). Molecular docking and simulation studies on SARS-CoV-2 M(pro) reveals Mitoxantrone, Leucovorin, Birinapant, and Dynasore as potent drugs against COVID-19. *Journal of Biomolecular Structure & Dynamics*, 1–12. Advance online publication. https://doi.org/10.1080/07391102.2020.1805019

Marchler-Bauer, A., Bo, Y., Han, L., He, J., Lanczycki, C. J., Lu, S., Chitsaz, F., Derbyshire, M. K., Geer, R. C., Gonzales, N. R., Gwadz, M., Hurwitz, D. I., Lu, F., Marchler, G. H., Song, J. S., Thanki, N., Wang, Z., Yamashita, R. A., Zhang, D., … Bryant, S. H. (2017). CDD/SPARCLE: Functional classification of proteins via subfamily domain architectures. *Nucleic Acids Research*, *45*(D1), D200–D203. https://doi.org/10.1093/nar/gkw1129

Mitchell, C. A., Ramessar, K., & O'Keefe, B. R. (2017). Antiviral lectins: Selective inhibitors of viral entry. *Antiviral Research*, *142*, 37–54. https://doi.org/10.1016/j.antiviral.2017.03.007

Murphy, P. V., André, S., & Gabius, H.-J. (2013). The third dimension of reading the sugar code by lectins: Design of glycoclusters with cyclic scaffolds as tools with the aim to define correlations between spatial presentation and activity. *Molecules (Basel, Switzerland)*, *18*(4), 4026–4053. https://doi.org/10.3390/molecules18044026

Nakagawa, Y., Doi, T., Taketani, T., Takegoshi, K., Igarashi, Y., & Ito, Y. (2013). Mannose-binding geometry of Pradimicin A. *Chemistry (Weinheim an Der Bergstrasse, Germany)*, *19*(32), 10516–10525. https://doi.org/10.1002/chem.201301368

Pinto, D., Park, Y.-J., Beltramello, M., Walls, A. C., Tortorici, M. A., Bianchi, S., Jaconi, S., Culap, K., Zatta, F., De Marco, A., Peter, A., Guarino, B., Spreafico, R., Cameroni, E., Case, J. B., Chen, R. E., Havenar-Daughton, C., Snell, G., Telenti, A., … Corti, D. (2020). Structural and functional analysis of a potent sarbecovirus neutralizing antibody. *BioRxiv*, 2020.04.07.023903. https://doi.org/10.1101/2020.04.07.023903

Rostock, M., Huber, R., Greiner, T., Fritz, P., Scheer, R., Schueler, J., & Fiebig, H. H. (2005). Anticancer activity of a lectin-rich mistletoe extract injected intratumorally into human pancreatic cancer xenografts. *Anticancer Research*, *25*(3B), 1969–1975.

Sato, H., Shewchuk, L. M., & Tang, J. (2006). Prediction of multiple binding modes of the CDK2 inhibitors, anilinopyrazoles, using the automated docking programs GOLD, FlexX, and LigandFit: An evaluation of performance. *Journal of Chemical Information and Modeling*, *46*(6), 2552–2562. https://doi.org/10.1021/ci600186b

Sauerborn, M. K., Wright, L. M., Reynolds, C. D., Grossmann, J. G., & Rizkallah, P. J. (1999). Insights into carbohydrate recognition by Narcissus pseudonarcissus lectin: The crystal structure at 2 A resolution in complex with alpha1-3 mannobiose. *Journal of Molecular Biology*, *290*(1), 185–199. https://doi.org/10.1006/jmbi.1999.2862

Sawada, Y., Numata, K., Murakami, T., Tanimichi, H., Yamamoto, S., & Oki, T. (1990). Calcium-dependent anticandidal action of Pradimicin A. *The Journal of Antibiotics*, *43*(6), 715–721. https://doi.org/10.7164/antibiotics.43.715

Sharma, A., & Vijayan, M. (2011). Influence of glycosidic linkage on the nature of carbohydrate binding in beta-prism I fold lectins: An X-ray and molecular dynamics investigation on banana lectin-carbohydrate complexes. *Glycobiology*, *21*(1), 23–33. https://doi.org/10.1093/glycob/cwq128

Singh, R., Bhardwaj, V., Das, P., & Purohit, R. (2020). Natural analogues inhibiting selective cyclin-dependent kinase protein isoforms: A computational perspective. *Journal of Biomolecular Structure & Dynamics*, *38*(17), 5126–5135. https://doi.org/10.1080/07391102.2019.1696709

Singh, R., Bhardwaj, V. K., Sharma, J., Das, P., & Purohit, R. (2020). Discovery and in silico evaluation of aminoarylbenzosuberene molecules as novel checkpoint kinase 1 inhibitor determinants. *Genomics*, S0888-7543(20)31960-1. Advance online publication. https://doi.org/10.1016/j.ygeno.2020.10.001

Swanson, M. D., Boudreaux, D. M., Salmon, L., Chugh, J., Winter, H. C., Meagher, J. L., André, S., Murphy, P. V., Oscarson, S., Roy, R., King, S., Kaplan, M. H., Goldstein, I. J., Tarbet, E. B., Hurst, B. L., Smee, D. F., de la Fuente, C., Hoffmann, H.-H., Xue, Y., … Markovitz, D. M. (2015). Engineering a therapeutic lectin by uncoupling mitogenicity from antiviral activity. *Cell*, *163*(3), 746–758. https://doi.org/10.1016/j.cell.2015.09.056

van der Meer, F. J. U. M., de Haan, C. A. M., Schuurman, N. M. P., Haijema, B. J., Peumans, W. J., Van Damme, E. J. M., Delputte, P. L., Balzarini, J., & Egberink, H. F. (2007). Antiviral activity of carbohydrate-binding agents against Nidovirales in cell culture. *Antiviral Research*, *76*(1), 21–29. https://doi.org/10.1016/j.antiviral.2007.04.003

van der Meer, F. J. U. M., de Haan, C. A. M., Schuurman, N. M. P., Haijema, B. J., Verheije, M. H., Bosch, B. J., Balzarini, J., & Egberink, H. F. (2007). The carbohydrate-binding plant lectins and the non-peptidic antibiotic Pradimicin A target the glycans of the coronavirus envelope glycoproteins. *The Journal of Antimicrobial Chemotherapy*, *60*(4), 741–749. https://doi.org/10.1093/jac/dkm301

Watanabe, Y., Allen, J. D., Wrapp, D., McLellan, J. S., & Crispin, M. (2020). Site-specific glycan analysis of the SARS-CoV-2 spike. *Science*, 369(6501), 330–333. https://doi.org/10.1126/science.abb9983

Yan, Y., Tao, H., He, J., & Huang, S. Y. (2020). The HDOCK server for integrated protein-protein docking. *Nature Protocols*, *15*(5), 1829–1852. https://doi.org/10.1038/s41596-020-0312-x

Zhao, P., Praissman, J. L., Grant, O. C., Cai, Y., Xiao, T., Rosenbalm, K. E., Aoki, K., Kellman, B. P., Bridger, R., Barouch, D. H., Brindley, M. A., Lewis, N. E., Tiemeyer, M., Chen, B., Woods, R. J., & Wells, L. (2020, July). Virus-receptor interactions of glycosylated SARS-CoV-2 spike and human ACE2 receptor. *BioRxiv: The Preprint Server for Biology*. https://doi.org/10.1101/2020.06.25.172403

Zhou, D., Tian, X., Qi, R., Peng, C., & Zhang, W. (2020). Identification of 22 N-glycosites on spike glycoprotein of SARS-CoV-2 and accessible surface glycopeptide motifs: Implications for vaccination and antibody therapeutics. *Glycobiology*, cwaa052. Advance online publication. https://doi.org/10.1093/glycob/cwaa052

Ziółkowska, N. E., O'Keefe, B. R., Mori, T., Zhu, C., Giomarelli, B., Vojdani, F., Palmer, K. E., McMahon, J. B., & Wlodawer, A. (2006). Domain-swapped structure of the potent antiviral protein Griffithsin and its mode of carbohydrate binding. *Structure (London, England: 1993)*, *14*(7), 1127–1135. https://doi.org/10.1016/j.str.2006.05.017